NATIONAL ADVISORY COMMITTEE FOR AERONAUTICS

TECHNICAL NOTE 4233

EXPERIMENTAL STUDY OF THE EQUIVALENCE OF TRANSONIC FLOW ABOUT SLENDER CONE-CYLINDERS OF CIRCULAR AND ELLIPTIC CROSS SECTION

By William A. Page

Ames Aeronautical Laboratory
Moffett Field, Calif.

Washington
April 1958

NATIONAL ADVISORY COMMITTEE FOR AERONAUTICS

TECHNICAL NOTE 4233

EXPERIMENTAL STUDY OF THE EQUIVALENCE OF TRANSONIC FLOW ABOUT SLENDER CONE-CYLINDERS OF CIRCULAR AND ELLIPTIC CROSS SECTION

By William A. Page

SUMMARY

This report describes an experimental investigation of the equivalence relationship and the related theory for lifting forces proposed by transonic slender-body theory. The models chosen for this study are a flat, winglike, elliptic cone-cylinder and its equivalent body of revolution, a circular cone-cylinder. It is determined that the flows about the two models are closely related in the manner predicted by the theory, the relationship persisting over a Mach number range of 0.92 to 1.05. Further, it is shown that the lifting forces on the elliptic cone-cylinder vary linearly only over the small angle-of-attack range of approximately $\pm 1^{\circ}$ and that the aerodynamic loading at sonic speed compares favorably with Jones' slender-wing theory.

The results of the investigation suggest that at transonic speeds and at small angles of attack the calculation of all aerodynamic characteristics of slender, three-dimensional shapes can be made by use of transonic slender-body theory when the pressures on the equivalent body of revolution are known, either by experiment, or by an adequate nonlinear theory. From transonic slender-body theory it is deduced that the slenderness required for this application is the same as that required for the successful application of the transonic area rule.

INTRODUCTION

The basic equations governing transonic flows with small perturbations have been well established. Techniques have been developed for solving the resulting nonlinear problem for the case of two-dimensional flows. The three-dimensional problem, however, has proven more formidable. Although solutions of the axisymmetric case have been developed, such as Yoshihara's cone-cylinder solution (ref. 1), and Oswatitsch's and Keune's approximate solutions for bodies of revolution (ref. 2), efforts to solve the more general problem of a three-dimensional shape, such as a wing-body combination, have led thus far only to the development of theories which relate solutions. An empirically developed relation is Whitcomb's transonic area

rule (ref. 3), which near the speed of sound equates the drag rise of a slender shape to the drag rise of a body of revolution having the same streamwise area distribution. Some theoretical justification for the application of this rule has been given by Harder and Klunker (ref. 4). Oswatitsch independently quoted his equivalence rule of transonic flow (refs. 5 and 6), which relates the flow about bodies with the same streamwise area distribution. Heaslet and Spreiter (ref. 7) have presented a formal transonic slender-body theory which relates the flow about a slender, three-dimensional object to the flow about its equivalent body. These theories extend the concepts of linearized slender-body theory to transonic speeds. The basic nonlinearity of the problem still remains, however, since the transonic solution to the flow about the equivalent body must still be determined.

It is the purpose of the present report to present the results of an experimental study of the transonic flow about a flat, winglike, elliptic cone-cylinder and its equivalent body of revolution, a circular cone-cylinder, with a view toward determining the applicability of transonic slender-body theory. The experimental data are studied first to see if the theoretically predicted equivalence relation actually occurs, second, to see if the range of applicability of the theory can be defined, and third, to see if the related theory for the lifting forces is applicable. To obtain the necessary experimental data for these purposes, the local pressures on the surface of an elliptic cone-cylinder and a circular cone-cylinder were measured in a transonic wind tunnel. These models were chosen for the investigation because their favorable pressure gradients would keep viscous effects to a minimum. Further, a slenderness condition was also fulfilled. The elliptic cone model was designed to simulate a slender, planar wing. The resulting value for the transonic similarity parameter, $A(t/l)^{1/3}$, was 0.78 which, it was concluded, would place the elliptic cone model in the family of triangular plan-form wings for which the transonic area rule is applicable (ref. 8).

SYMBOLS

A	aspect ratio
C_p	pressure coefficient, $\frac{p-p_\infty}{q_\infty}$
ΔC_p	difference in pressure coefficient across wing, $C_{p_l} - C_{p_u}$
h	half-tunnel height
l	length of conical part of models
m	tangent of the semiapex angle of the wing plan form
M_∞	free-stream Mach number

p	static pressure
p_∞	free-stream static pressure
q_∞	free-stream dynamic pressure, $\frac{1}{2}\rho_\infty U_\infty^2$
r	body radius
s	wing span
$S(x)$	streamwise area distribution
t	maximum wing thickness
U_∞	free-stream velocity
x,y,z	longitudinal, lateral, and normal coordinate system
α	angle of attack, deg
η	$\sin^{-1}\frac{y}{mx}$
ρ_∞	free-stream density
φ	perturbation potential

Subscripts

2	two-dimensional
B	body
l	lower surface
t	due to thickness
u	upper surface
W	wing
x,y,z	derivative with respect to x, y, or z
α	due to angle of attack

Superscript

$*$	conditions at the sonic point

APPARATUS

The experimental study was made in the Ames 2- by 2-foot transonic wind tunnel, which is of the closed-circuit, variable-pressure type. The wind tunnel is fitted with a flexible nozzle followed by a ventilated test section of 6-percent open area which permits continuous choke-free operation from 0 to 1.4 Mach number. For a more detailed description of the tunnel, see reference 9. Condensation effects are rendered negligible by maintaining the air in the tunnel at a specific humidity of less than 0.0003 pound of water per pound of air.

Dimensional details of the models are shown in figure 1. Both models were constructed of steel.

The triangular portion of the plan form of the elliptic cone-cylinder is of aspect ratio 2 and thickness ratio 6 percent. Cross sections of the elliptic cone-cylinder model taken normal to the x axis or flight direction at zero angle of attack are all ellipses with the minor axis equal to 6 percent of the major axis. The afterportion of the model was constructed so as to preserve a constant cross-sectional area distribution as the wing changed from an elliptic to a circular cross section for attachment to the wind-tunnel support sting. This afterbody design was expected to reduce flow disturbances that might propagate upstream at high subsonic Mach numbers.

The circular cone model was constructed to have the same longitudinal area distribution as the elliptic cone model. This required that the cone half-angle be $6^{\circ}59'$. The afterportion of the model is a circular cylinder with a constant cross-sectional area distribution.

Surface pressures were determined on both models by means of 0.016-inch-diameter orifices located on one side of each model at the positions listed in figure 1. Orifices were placed in only one surface of the elliptic cone-cylinder in order to simplify the design and construction of the model. As indicated in figure 1, however, additional orifices were provided in the opposite side of both the circular and elliptic cone models to provide a check on the angle-of-attack settings. All orifices led directly to internally located stainless-steel tubes which emerged from the interior of the models at the rear. The tubes were connected to a multiple-tube manometer utilizing tetrabromoethane (specific gravity 2.97) as the measuring fluid.

Support for the models in the test section of the wind tunnel was provided by a 1-inch-diameter sting as shown in figure 2. The models blocked 0.25 percent of the test-section cross-sectional area.

TESTS

The test program consisted of the measurement of the pressure distribution on the circular and elliptic cone models at zero angle of attack, the measurement of the pressure distribution on the elliptic cone when at angle of attack, and a special test consisting of the measurement of the pressure distribution on the circular cone model at zero angle of attack in a larger transonic wind tunnel, the Ames 14-foot transonic wind tunnel. This latter test was performed to evaluate the magnitude and extent of possible wall interference in the 2- by 2-foot transonic wind tunnel.

Since a complete set of orifices was present in only one surface of the elliptic cone-cylinder, it was necessary, in order that complete data might be obtained, to test at both positive and negative angles of attack. Pressures on the model surface were recorded by photographing the manometer. Two photographs of the manometer were taken at each test condition, one when it was judged the pressures had reached equilibrium and the other approximately one minute later. When the data were reduced it was discovered that in the majority of the comparisons the two photographs were identical. For the cases where differences occurred, the second of the two readings was used to reduce the data.

Determination of the free-stream Mach number in the wind-tunnel test section was made by (1) assuming isentropic flow between the tunnel reservoir and test section and (2) measuring the total pressure in the reservoir and the static pressure in the plenum chamber that surrounds the porous-walled test section. It has previously been determined (ref. 9) that the static pressure in the plenum chamber is equal to the empty tunnel free-stream static pressure at the model location. The Reynolds number of the test was held constant at 2.4×10^6, based upon the 5.50-inch length of the conical part of the models.

REDUCTION AND PRECISION OF DATA

The static pressures measured at the orifices on the surface of the models were reduced to standard pressure-coefficient form, C_p. The angles of attack at which the data are presented have been corrected for the elastic deflection of the model and support sting.

Certain random errors of measurement exist which determine the precision or repeatability of the data. An analysis of the precision of the Mach number, angle of attack, and pressure coefficient has been made and the random uncertainties at three representative Mach number are listed below:

	$M_\infty = 0.8$	$M_\infty = 1.0$	$M_\infty = 1.2$
M_∞	±0.003	±0.004	±0.002
α	±.1	±.1	±.1
C_p	±.002	±.002	±.002

The experimental data in the transonic range were influenced by wind-tunnel-wall interference. An evaluation and discussion of the interference on the circular cone-cylinder at zero angle of attack is given in the appendix. Wall interference at angle of attack was not evaluated. Even though this study shows interference to be present, it is assumed, for reasons stated in the appendix, that the comparisons made to evaluate the equivalence relationship are valid.

SUMMARY OF TRANSONIC SLENDER-BODY THEORY

The following section describes, in a simple manner, the transonic slender-body theory that is under experimental investigation herein. Perhaps the simplest method of presenting the theory, the approximations involved, and the expected limitations is first to describe the closely related and well-developed theory of slender wing-body combinations at subsonic and supersonic speeds as developed by Jones (ref. 10), Ward (ref. 11), and Heaslet and Lomax (ref. 12).

If the assumption is made that the body, wing, or wing-body combination under consideration is slender in the streamwise direction, and if attention is focused on the flow field in the vicinity of the configuration, the perturbation potential is given by the relation

$$\varphi = \varphi_2 + f(x) \tag{1}$$

The above equation states that the perturbation potential about a slender three-dimensional object flying at either subsonic or supersonic speeds is approximated in the vicinity of the configuration by the sum of two potential fields. The first term, φ_2, is the solution to the two-dimensional Laplace equation and the boundary conditions in transverse planes, while the second term, $f(x)$, is dependent solely upon the streamwise gradient of area of the configuration.

The basic ideas of the slender-body approximation delineated above have been applied to the nonlinear transonic flow equation by Harder and Klunker (ref. 4), Oswatitsch and Keune (refs. 5 and 6), and Heaslet and Spreiter (ref. 7). Harder and Klunker derived the expression

$$\varphi = \varphi_2 + g(x) \tag{2}$$

which is of the same form as given in equation (1), but with the important difference that the unknown function $g(x)$ now replaces the previously

known $f(x)$. One of the properties of $g(x)$, identical to that of $f(x)$, is that it depends solely upon the streamwise area distribution, and thus will be the same for a slender wing and its equivalent body of revolution.

Oswatitsch's equivalence rule of transonic flow may be stated as follows: "The solution for transonic flow around a thin, nonlifting, low-aspect-ratio wing can be obtained from that for a nonlifting body of revolution having the same longitudinal distribution of cross-sectional area by superposing the difference between the two-dimensional harmonic crossflow solutions for the two bodies." It is to be noted that the equivalence rule and the equations above actually express the same fundamental concept.

A complete analysis of slender-body theory at transonic speeds has been given by Heaslet and Spreiter (ref. 7). Equation (2) is also obtained from their formal analysis, but with important additional information. It is shown that the relative error made in neglecting the next highest term in the analysis is of order (ts^3/l^4). Furthermore, the slender-wing theory of Jones is shown to be the applicable theory for computing lifting forces, with the additional condition that the angle of attack must be small. This condition is caused by a coupling between the effects of thickness and angle of attack which becomes pronounced when the angle of attack is the order of magnitude of the thickness ratio.

As to the degree of slenderness required for the application of the theoretical relations described above, it can be reasoned that since the transonic area rule is also predicted by equation (2), any limitation to the application of the area rule would also reflect a limitation to the application of the above theory. Limitations to the transonic area rule have been defined experimentally in a few cases (e.g., refs. 8 and 13). Hence, it can be concluded that these limitations also apply to further applications of the relation expressed by equation (2).

The expected usefulness of equation (2) lies in its application to slender three-dimensional shapes flying at transonic speeds. If the equation is written twice, once for the slender shape (say, a wing), once for the equivalent body, and then one subtracted from the other, there is obtained

$$\varphi_W = \varphi_{2_{W_t}} + \varphi_{2_{W_\alpha}} - \varphi_{2_B} + \varphi_B \tag{3}$$

where φ_{2_W} is shown as having contributions from both the thickness and the angle of attack of the wing. The first three terms on the right of the equation are two-dimensional crossflow potentials and can be obtained from solutions of Laplace's equation, $\varphi_{yy} + \varphi_{zz} = 0$. The last term on the right is the full transonic solution for the body and must be obtained from a solution of the transonic small-disturbance equation or from experiment. Since the purpose of the present report is to investigate experimentally the equivalence relationship, it is pertinent to write equation (3)

in terms of pressure coefficients. The derivation of the expression for pressure coefficient from the potential equation is given for planar shapes in reference 7. The expression is

$$C_{p_W} = C_{p_B} - \frac{2}{U_\infty}\frac{\partial}{\partial x}\varphi_{2_W} + \frac{S_{xx}(x)}{2\pi}\ln\frac{S(x)}{\pi} + \frac{[S_x(x)]^2}{4\pi S(x)} \tag{4}$$

where the remaining two-dimensional potential term $\frac{\partial}{\partial x}\varphi_{2_W}$ is obtained as noted before, and $S(x)$ is the streamwise area distribution of the equivalent body. The pressure coefficient, C_{p_B}, refers to the values at the surface of the equivalent body. It is seen, therefore, that if the pressure coefficient on a slender body is known at transonic speeds, the pressure coefficient and, correspondingly, the aerodynamic forces can be determined on any slender object that has the same streamwise distribution of area as that of the body.

To specialize equation (4) to the models under investigation, we write for the longitudinal area distribution of the elliptic cone,

$$S(x) = \frac{\pi t m x^2}{2l} \tag{5}$$

where m is the tangent of the plan-form semiapex angle, l is the length of the conical portion of the model, and t is the maximum thickness. The crossflow potential, φ_{2_W}, is determined for the nonlifting planar case from the expression

$$\varphi_{2_W} = \frac{1}{2\pi}\int_{mx}^{-mx} 2U_\infty \frac{\partial}{\partial x} Z_u(x,y_1)\ln[(y-y_1)^2+z^2]^{1/2}dy_1 \tag{6}$$

where $\frac{\partial}{\partial x} Z_u$ is the surface slope of the elliptic cone given by

$$\frac{\partial}{\partial x} Z_u = \frac{mtx}{2l(m^2x^2-y^2)^{1/2}} \tag{7}$$

Evaluation of equation (6) in the $z = 0$ plane yields for the crossflow potential

$$\varphi_{2_W} = \frac{U_\infty t m x}{2l}\ln\frac{mx}{2} \tag{8}$$

Combining equations (5) and (8) in equation (4), one obtains for the surface pressure coefficient on the elliptic cone

$$C_{p_W} = C_{p_B} - \frac{mt}{2l}\left(1+\ln\frac{ml}{2t}\right) \tag{9}$$

For our elliptic cone, for which $m = 1/2$, and $t/2l = 0.03$, equation (9) reduces to

$$C_{p_W} = C_{p_B} - 0.0364 \tag{10}$$

where C_{p_B} is obtained on the surface of the equivalent circular cone-cylinder body of revolution which has a half-angle of $6^{\circ}59'$.

A more exact representation of the zero-lift pressures on the elliptic cone can be obtained by satisfying the boundary conditions for the determination of the crossflow potential at the surface of the elliptic cone instead of in the $z = 0$ plane. Such a crossflow solution for the elliptic cone is presented in reference 14 for linearized slender-body theory. This solution can be utilized for the present purposes, and, after some reduction, there is obtained

$$C_{p_W} = C_{p_B} + m\left(\frac{t}{2l}\right)\ln\frac{4m(t/2l)}{(m+t/2l)^2} - m\left(\frac{t}{2l}\right) + \frac{m^2(t/2l)^2}{m^2\sin^2\eta+(t/2l)^2\cos^2\eta} \tag{11}$$

where $\eta = \sin^{-1}y/mx$. Along the center line, where $y = 0$, this more exact expression predicts for the elliptic cone of $m = 1/2$, $t/2l = 0.03$,

$$C_{p_W} = C_{p_B} - 0.0372 \tag{12}$$

as contrasted to the previous expression (10) for the planar case. Thus, it is seen that the difference along the center line is small. At the leading edge, however, where $y = mx$, equation (11) predicts a partial stagnation pressure of magnitude

$$C_{p_W} = C_{p_B} + 0.212 \tag{13}$$

which the planar boundary condition case does not predict, since equation (10) applies everywhere on the surface.

RESULTS AND DISCUSSION

The experimental data obtained during the course of the investigation are presented in two forms. A large portion of the data is tabulated and can be found in table I. Selected portions of these data are subsequently presented in graphical form to evaluate various phases of the transonic slender-body theory described previously. The data at zero angle of attack

are examined to see if the equivalence relationship proposed by the theory is valid at sonic speed. The data at Mach numbers other than 1 are studied to determine the range of speeds about $M_\infty = 1.0$ for which the equivalence relationship holds. Further, the lifting pressures on the elliptic cone model are examined and compared with existing theories for the angle-of-attack case.

Flow Equivalence at Sonic Speed

From the previous discussion of the transonic slender-body theory it is to be expected that a marked similarity should exist between the pressure coefficients observed on the two test models at sonic speed. In fact, equation (10) from the previous section indicates that the data should differ by a fixed constant. It is also possible to predict the pressure coefficient on the elliptic cone by adding this same constant to the data from the circular cone-cylinder, calling the resultant values the "equivalence prediction" of the pressures on the elliptic cone. Figure 3 shows the experimental pressure distribution on the two test models for $M_\infty = 1.0$. The data for the elliptic cone are shown for the center line where $y/mx = 0$. Also included in the figure is the equivalence prediction derived as described above. Inspection of the figure shows remarkable agreement between the elliptic cone data and the "prediction" from the theory, thus indicating the validity of the equivalence relationship. It can be noted that the only basic difference in the two curves appears just upstream of the cone shoulder. At first thought, one might attribute this difference to viscous effects, but this is not necessarily the case. It must also be remembered that the basic theory being used (i.e., transonic slender-body theory) is applicable only to smooth slender shapes. The theory is therefore suspect at the cone shoulder, since at this location the body is not smooth.

Figure 4 compares the equivalence predictions with the data in planes normal to the free-stream direction at three representative values of x/l. Two different predictions are shown. One, labeled "planar approximation," is identical to the form described in reference 7 (i.e., eq. (10) herein), while the other, labeled "exact boundary condition," is obtained by satisfying the boundary conditions on the surface of the elliptic cone instead of in the $z = 0$ plane (eq. (11)). The two solutions differ appreciably only in the vicinity of the edge. Inspection of the figure illustrates again that the agreement between the slender-body prediction and the pressure coefficient on the elliptic cone is excellent except in the vicinity of the shoulder where the disagreement is now seen to extend out to the edge of the elliptic cone. It is suspected that the major reason for disagreement in this region lies in slenderness restrictions basic to the derivation of the theory. Not only is it possible that the elements of the elliptic cone extend too far from the axis of symmetry for the theory to apply with complete uniformity, but, as mentioned before, the shoulder of the elliptic cone-cylinder has an unsmooth character.

Mach Number Range of Equivalence

Since transonic slender-body theory, in essence, is an extension to transonic speeds of the well-known linearized slender-body theory of Ward and Jones, it is to be expected that the equivalence of the flows, demonstrated for a Mach number of 1 in the previous section, will extend into the subsonic and supersonic speed ranges. In fact, the controlling parameter, as we move away from a Mach number of 1, is the slenderness of the object under consideration. This can be seen more clearly from an examination of the order of the error term in the expressions for the potential about the wing as given in reference 7. In the linearized case the error term has the form $(M_\infty^2-1)O[(ts^3/l^4)\ln s]$, whereas in the sonic case the form is $O[(t^2s^4/l^6)\ln s]$. Since the span, s, is raised to a higher power in the expression for sonic speed, the slenderness requirement becomes more restrictive as the Mach number increases or decreases from a value of 1. Thus, it is to be expected that the equivalence predictions of the present investigation will agree best with the elliptic cone data for a small range of Mach numbers about sonic speed.

This expected behavior is shown in figure 5 which presents typical results from a few selected points on the elliptic cone surface. At a value of x/l equal to 0.7 and at values of y/mx equal to 0 and 0.67, good agreement between the elliptic cone data and the equivalence-rule prediction extends over a Mach number range of approximately 0.92 to 1.05. Outside this range, the equivalence prediction deviates from the elliptic cone data, the difference increasing as the Mach number becomes further removed from 1. At other points further forward on the elliptic cone, the same general behavior is apparent, although perhaps not so pronounced. At the rear of the elliptic cone, however, there is little agreement between the data and the equivalence prediction, a situation similar to that encountered near the cone shoulder when the data were compared with the equivalence prediction at sonic speed in the preceding section of this report. In general, the comparisons of figure 5 show that the elliptic cone model of this investigation, with a value of $A(t/l)^{1/3}$ equal to 0.78, is sufficiently slender for the equivalence relationship to hold over a Mach number range of approximately 0.92 to 1.05. Above this Mach number range, more accurate predictions of the surface pressures should be obtained from Van Dyke's second-order slender-body theory (ref. 14). It is to be noted in figure 5 that the second-order-theory predictions, while not in exact agreement with the experimental results, are somewhat superior to those of the transonic slender-body theory.

Lifting Pressures at Transonic Speeds

The discussion of transonic slender-body theory included in a previous section does not specify a relationship between the lifting forces on a slender wing and its equivalent body. Instead, it is pointed

out that the lifting forces on the wing are to be estimated by use of the well-known slender-wing theory of Jones (ref. 10), which depicts the flow as that about a translating flat plate in an incompressible flow field. However, the restriction derived by the analysis given in reference 7 is that slender-wing theory applies only if the angle of attack of the wing is small compared with the thickness ratio.

Since slender-wing theory predicts a linear variation of pressure coefficient with angle of attack, figure 6 has been prepared to show the experimental angle-of-attack range over which a linear relationship holds. The pressure coefficients at a few selected points on the elliptic cone surface are plotted as a function of angle of attack at a Mach number of 1. Included in the figure is the calculated variation of surface pressure coefficient with angle of attack as obtained from slender-wing theory. Inspection of the figure shows that near zero angle of attack, the range of linear variation is quite small, being on the order of a few degrees. At positive angles of attack (pressures were measured on the upper surface of the elliptic cone), an abrupt change in the variation of pressure coefficient with angle of attack occurs at $\alpha = 1/2^\circ$ to 1°. At negative angles, the deviation from linearity is less abrupt, and occurs slowly, making it difficult to call out a definite value of angle of attack where the linear variation breaks down. In general, the deviation becomes noticeable at $\alpha = -2^\circ$ or -3°. Since the aerodynamic loading is given by the difference in pressure across the wing surface, it can be concluded, that for the present elliptic cone, the range of applicability of slender-wing theory at sonic speed is restricted to an angle-of-attack range of approximately $\pm 1^\circ$. The effective wing thickness for this angle-of-attack range, considered in terms of the surface slope change swept out by the $y/mx = 0$ generator of the elliptic cone surface, can be represented by a slope of 0.0175, compared with the actual slope of the elliptic cone surface of 0.03. Therefore, at sonic speed, the angle-of-attack range over which the slender-wing theory is strictly applicable appears to be smaller than the thickness ratio of the wing.

In order to illustrate further the applicability of slender-wing theory to the aerodynamic loading at sonic speed on the elliptic cone, figure 7 has been prepared to show the variation of $d(\Delta C_p)/d\alpha$ at zero angle of attack. Part (a) of the figure shows the variation along the line of symmetry ($y/mx = 0$) of the elliptic cone, while part (b) illustrates the variation along the span at three longitudinal positions. Included in the figure are the predictions of slender-wing theory. The agreement between experiment and theory, in general, is good, particularly in the spanwise direction. Again, the most significant difference occurs in the vicinity of the elliptic cone shoulder, the location where the greatest differences between theory and experiment have been noted previously.

In the section on the behavior of the surface pressures on the elliptic cone at zero angle of attack, it was demonstrated that the data deviated from the equivalence prediction at Mach numbers above and below a Mach number of 1. The slenderness requirement for the application of

transonic slender-body theory was thus shown to become more restrictive as the free-stream velocity increases or decreases from sonic speed. A similar slenderness restriction is expected to apply for the aerodynamic loading when estimated by slender-wing theory.

The variation of $d(\Delta C_p)/d\alpha$ as a function of Mach number is shown graphically for a few selected points on the elliptic cone surface in figure 8. The slender-wing-theory prediction, which is invariant with Mach number and plots as a horizontal line, is included. There are two significant effects that can be noted from an examination of the figure. First, at transonic speeds, a small amount of wind-tunnel interference is apparently present; note particularly the abrupt changes in the magnitude of the experimental loading at Mach numbers between 1.02 and 1.10. Second, inspection of the magnitude of the experimental loading over most of the elliptic cone surface indicates that slender-wing theory is valid for only a small range of Mach numbers about sonic speed. At supersonic speeds for instance, a better prediction of the aerodynamic loading can be made by the linear-theory calculations of reference 15 for lifting triangular wings. The predicted variation of $d(\Delta C_p)/d\alpha$, which now depends upon the Mach number, has also been included in figure 8. The supersonic data from the elliptic cone are in better agreement with this more exact theory at the higher test Mach numbers.

An additional and very interesting prediction can also be made regarding the change of aerodynamic loading with Mach number in the immediate vicinity of sonic speed by applying the concept of the "Mach number freeze" (see, e.g., ref. 16, p. 275) to the lifting pressures. The term "Mach number freeze" means the invariance of local Mach number with free-stream Mach number. The rule for the freezing of the local Mach number in terms of the rate of change of pressure coefficient with Mach number is given by

$$\left(\frac{dC_p}{dM_\infty}\right)_{M_\infty=1.0} = \frac{4}{\gamma+1} - \frac{2}{\gamma+1}\,(C_p)_{M_\infty=1.0} \tag{14}$$

Application to the aerodynamic loading gives

$$\Delta C_p = C_{p_l} - C_{p_u}$$

$$\frac{d(\Delta C_p)}{dM_\infty} = \frac{dC_{p_l}}{dM_\infty} - \frac{dC_{p_u}}{dM_\infty}$$

$$\left[\frac{d(\Delta C_p)}{dM_\infty}\right]_{M_\infty=1.0} = -\frac{2}{\gamma+1}\left(C_{p_l} - C_{p_u}\right)_{M_\infty=1.0} = -\frac{2}{\gamma+1}\,(\Delta C_p)_{M_\infty=1.0}$$

$$\left[\frac{d^2(\Delta C_p)}{dM_\infty d\alpha}\right]_{\substack{\alpha=0\\ M_\infty=1.0}} = -\frac{2}{\gamma+1}\left[\frac{d(\Delta C_p)}{d\alpha}\right]_{\substack{\alpha=0\\ M_\infty=1.0}} \tag{15}$$

In order to compare this prediction with the experimental loading observed on the elliptic cone, the rate of change of $d(\Delta C_p)/d\alpha$ with Mach number as given by equation (15) has been added to figure 8. The figure shows that the experimental data tend to agree with the prediction on the forward portion of the cone surface, but do not agree on the afterportion. It can be supposed that the gentle "hump" in the value of the experimental loading at Mach numbers just below 1 is a real free-air phenomenon and is a manifestation of the Mach number freeze, although it must be emphasized that the data are not necessarily free of wind-tunnel wall interference. Nevertheless, the results of the above comparison suggest that contrary to slender-wing theory, the rate of change of $d(\Delta C_p)/d\alpha$ with Mach number varies in the immediate neighborhood of sonic speed in the manner shown.

CONCLUDING REMARKS

In the present report, transonic slender-body theory has been experimentally evaluated for the case of a flat, winglike, elliptic cone-cylinder and its equivalent body of revolution, a circular cone-cylinder. Emphasis has been placed upon answering three questions; namely, (1) does the equivalence relationship given by transonic slender-body theory adequately relate the actual flows, (2) can its range of applicability be defined, and (3) does the related lifting theory adequately describe the aerodynamic loading on the elliptic cone?

Experimentally, it was determined that the flow at transonic speeds about a circular cone-cylinder and an elliptic cone-cylinder are closely related in the manner predicted by transonic slender-body theory. For the elliptic cone chosen for the test, with a value of the transonic similarity parameter which describes slenderness, $A(t/l)^{1/3}$, equal to 0.78, the equivalence of the flows between the elliptic cone and its equivalent body persists over a Mach number range from 0.92 to 1.05. The pressures in the shoulder region of the model deviate somewhat from the predictions derived from the theory because, it is thought, of the unsmooth character of the shoulder. The lifting forces on the elliptic cone vary linearly only over the small angle-of-attack range of approximately $\pm 1^{\circ}$, a result not inconsistent with the theory, since this angle-of-attack range represents a thickness ratio less than the actual thickness. Further, the aerodynamic loading at sonic speed compares favorably with Jones' slender-wing theory, the only significant deviations occurring again in the shoulder region. At subsonic and supersonic speeds, the aerodynamic loading varies sufficiently with Mach number that slender-wing theory no longer appears adequate. However, at supersonic speeds, the decrease in loading observed with increasing Mach number is well predicted by linear theory.

The results of the present investigation suggest that at transonic speeds and at small angles of attack the calculation of all aerodynamic

characteristics of slender, three-dimensional shapes can be made by use of transonic slender-body theory when the pressures on the equivalent body are known, either by experiment, or by an adequate nonlinear theory. From transonic slender-body theory it is deduced that the slenderness required for this application is the same as that required for the successful application of the transonic area rule.

Ames Aeronautical Laboratory
National Advisory Committee for Aeronautics
Moffett Field, Calif., Jan. 7, 1958

APPENDIX

WIND-TUNNEL INTERFERENCE AT TRANSONIC MACH NUMBERS

For the determination at transonic speeds of the general aerodynamic forces on bodies, wings, and wing-body combinations, the three-dimensional porous-walled transonic wind tunnel has been widely used and has proven to be a valuable research tool. It is recognized, however, that interference effects exist, generally depending upon the size of the model with respect to the tunnel - the smaller the model, the smaller the interference effects. Three general forms of interference are known to exist, (1) subsonic interference which depends upon the volume of the model, and which may become significant as the Mach number approaches high subsonic values, (2) transonic interference, which depends upon the length and fineness ratio of the model, and (3) supersonic, or wave reflection interference, caused primarily by the presence of the attenuated reflection of the model bow shock wave from the test-section walls. This latter interference effect begins at Mach numbers slightly above 1 and terminates as soon as the reflected disturbances pass off the afterportion of the model.

With these considerations in mind it was deemed necessary to assess the suitability of the test facility for obtaining accurate data on the test configurations of this investigation at transonic speeds. To evaluate the importance of the interference effects in the 2- by 2-foot transonic wind tunnel the circular cone-cylinder model was also tested in a much larger transonic tunnel, the Ames 14-foot transonic wind tunnel, where the blockage ratio of the model was less by a factor of nearly 50, 0.005 percent compared to 0.25 percent of the tunnel cross-sectional area. The test setup and procedure in the 14-foot tunnel were essentially identical to those used in the 2- by 2-foot tunnel.

A comparison of the results obtained from the two test facilities is given in figures 9 and 10. Figure 9 shows the pressure coefficient obtained at a Mach number of 1 on the circular cone-cylinder model at the two blockage ratios. Also included in the figure is Yoshihara's theoretical solution (ref. 1) for the circular cone-cylinder at a Mach number of 1. (Yoshihara's results have been corrected for an error in the sign of the squared term in the pressure coefficient.) The theoretical solution has been adjusted by use of the transonic similarity parameters for bodies of revolution (ref. 17) from a cone half-angle of 10° as used by Yoshihara to the present cone half-angle of $6^\circ 59'$. Inspection of the figure shows that the level of the experimental pressure coefficients from the two test facilities differs by as much as 14 percent, whereas the theoretical curve has fundamentally a different shape - although the average level of the theoretical pressure coefficient is in better agreement with the data from the larger wind tunnel.

A further comparison between the data from the two test facilities is shown in figure 10. Here, the pressure coefficient as measured at one of

the orifice locations ($x/l = 0.486$) is plotted as a function of Mach number. Included in the figure is the exact theoretical pressure coefficient at supersonic Mach numbers as interpolated from the Kopal tables (ref. 18), and the linearized theory pressure coefficient at subsonic Mach numbers as given by Laitone (ref. 19). The effects shown are typical of those occurring at other locations on the cone surface. As an additional point of interest there is included in the figure the rate of change of pressure coefficient with Mach number, dC_p/dM_∞, at a Mach number of 1 that represents the invariance of local Mach number with free-stream Mach number. This so-called Mach number freeze has been discovered on two-dimensional wings at transonic Mach numbers by other investigators and apparently is a phenomenon basic to transonic flows in general.

Inspection of figure 10 indicates that the Mach number range where the data from the two facilities differ and where wind-tunnel wall interference apparently exists extends approximately from 0.99 to 1.05. It would appear from consideration of the small size of the cone-cylinder model in the larger wind tunnel that the data shown from this facility are essentially interference free. However, an unpublished analysis for circular, porous-walled, transonic wind tunnels, similar to that given by Berndt in reference 20 for slotted tunnels, indicates that the Mach number error due to wall interference at sonic speed is given by

$$\Delta M = -0.82(r^*/h)^{6/7}(r^*/x^*)^{2/7}$$

$$M_\infty = 1 - \Delta M$$

where M_∞ is the indicated Mach number in the wind tunnel, h is the half-tunnel height, and x^* and r^* are the coordinates of the sonic point on the body surface. The equation is derived for the case of vanishingly small model size and for a slowly varying wall permeability with longitudinal distance. However, application to the present facilities indicates that sonic free air conditions are simulated in the wind tunnel when the measured Mach number is 1.035 for the small facility and 1.0066 for the large facility. Figure 11 has been prepared to illustrate the effect of this Mach number correction on the experimental data obtained from the two test facilities. The data from both facilities at the simulated sonic free air conditions now appear to be nearly in perfect agreement, except over the forward portion of the cone. Since the correction formula developed above is based upon a vanishingly small model size, it is thought that the discrepancy is due to a Mach number gradient caused by the large size of the model in the smaller facility.

A further point of interest is to note, that even though ΔM for the larger facility is small, being only 0.0066, the pressure coefficient at the simulated sonic free air condition is some 8 percent higher than the value at the indicated sonic speed in the wind tunnel.

To illustrate further the presence of wind-tunnel wall interference, the series of schlieren photographs shown in figure 12 have been included. Photographs taken at the same Mach number from the two test facilities are shown one above the other. At a Mach number of 0.96 the shock-wave patterns are essentially identical. Note that the terminal shock (i.e., the shock wave located just aft of the cone shoulder) does not reach all the way to the test-section walls of the small facility. At higher Mach numbers, substantial differences in the shock pattern begin to occur. It is in this Mach number range that the measurements of pressures on the model surface (fig. 10) begin to show significant differences between the two facilities. Note particularly that at a Mach number of 1.0 the location of the terminal shock is widely different; for a blockage ratio of 0.25 percent, it is located along the cylindrical portion of the model, whereas for a blockage ratio of 0.005 percent, it is located downstream of the model. The location of this shock pattern is believed to be determined primarily by the impingement of the expansion field from the cone shoulder on the walls of the wind-tunnel test section. Although the different shock pattern on the afterportion of the model is the only manifestation of wall interference at $M_\infty = 1.0$ that can be seen in the photographs, the pressure distribution shown in figure 9 indicates the presence of a strong interference field over the conical portion of the model. In fact, the interference correction formula presented earlier in the appendix suggests that schlieren pictures at $M_\infty = 1.0066$ in the larger facility and at $M_\infty = 1.035$ in the smaller facility should show similar flow fields. The closest available comparison is for $M_\infty = 1.00$ in the upper row and $M_\infty = 1.04$ in the lower row of the photographs of figure 12. Even this comparison does not tend to show similar flow fields which further illustrates the fact that the interference correction formula developed is not sufficiently accurate for the model size used in the small facility. At slightly higher supersonic Mach numbers ($M_\infty = 1.06$ and 1.10), the pairs of schlieren photographs indicate, as do the pressure coefficients shown in figure 10, that the flow field in the vicinity of the model is essentially the same in either tunnel.

In summary, the above comparisons have shown that the absolute accuracy of the pressure coefficient at transonic speeds obtained on a slender cone at a blockage ratio of 0.25 percent is poor. It can be reasoned, however, that since interference errors depend upon the length, volume, and fineness ratio of the test model and are little influenced by the details of the model cross-sectional shape (refs. 20 and 21), the relative comparisons of pressure-coefficient data from the circular cone and the elliptic cone at the same blockage ratio of 0.25 percent will be valid. It is with this assumption that the data of this investigation have been presented, since at transonic speeds the equivalence comparisons made are all completely relative in nature.

REFERENCES

1. Yoshihara, Hideo: On the Flow Over a Cone-Cylinder Body at Mach Number One. WADC Tech. Rep. 52-295, Nov. 1952.

2. Oswatitsch, K., and Keune, F.: The Flow Around Bodies of Revolution at Mach Number 1. Proc. Conf. on High-Speed Aeronautics, Polytechnic Inst. of Brooklyn, N. Y., Jan. 20-22, 1955, pp. 113-131.

3. Whitcomb, Richard T.: A Study of the Zero-Lift Drag-Rise Characteristics of Wing-Body Combinations Near the Speed of Sound. NACA Rep. 1273, 1956. (Supersedes NACA RM L52H08)

4. Harder, Keith C., and Klunker, E. B.: On Slender-Body Theory at Transonic Speeds. NACA TN 3815, 1956. (Supersedes NACA RM L54A29a)

5. Oswatitsch, K.: Die Theoretischen Arbeiten Uber Schallnahe Stromungen am Flugtechnischen Institut der Kungl. Tekniska Högskolam, Stockholm. Proc. of Eight Int. Cong. on Theo. and Appl. Mech., 1953, pp. 261-262.

6. Oswatitsch, Klaus, and Keune, Friedrich: Ein Äquivalenzsatz für Nichtangestellte Flügel Kleiner Spannweite in Schallnaher Strömung. Zeitschrift für Flugwissenschaften, 3 Jahrgang, Heft 2, Feb. 1955, S. 29-46.

7. Heaslet, Max. A., and Spreiter, John R.: Three-Dimensional Transonic Flow Theory Applied to Slender Wings and Bodies. NACA TN 3717, 1956.

8. Page, William A.: Experimental Determination of the Range of Applicability of the Transonic Area Rule for Wings of Triangular Plan Form. NACA TN 3872, 1956.

9. Spiegel, Joseph M., and Lawrence, Leslie F.: A Description of the Ames 2- by 2-Foot Transonic Wind Tunnel and Preliminary Evaluation of Wall Interference. NACA RM A55I21, 1956.

10. Jones, Robert T.: Properties of Low-Aspect-Ratio Pointed Wings at Speeds Below and Above the Speed of Sound. NACA Rep. 835, 1946. (Supersedes NACA TN 1032)

11. Ward, G. N.: Supersonic Flow Past Slender Pointed Bodies. Quart. Jour. Mech. and Appl. Math., vol. 2, pt. 1, 1949, pp. 75-97.

12. Heaslet, Max. A., and Lomax, Harvard: The Calculation of Pressure on Slender Airplanes in Subsonic and Supersonic Flow. NACA Rep. 1185, 1954. (Supersedes NACA TN 2900)

13. Spreiter, John R.: On the Range of Applicability of the Transonic Area Rule. NACA TN 3673, 1956. (Supersedes NACA RM A54F28)

14. Van Dyke, Milton D.: The Slender Elliptic Cone as a Model for Nonlinear Supersonic Flow Theory. Jour. Fluid Mech., vol. 1, May 1956, pp. 1-15.

15. Brown, Clinton E.: Theoretical Lift and Drag of Thin Triangular Wings at Supersonic Speeds. NACA Rep. 839, 1946. (Supersedes NACA TN 1183)

16. Liepmann, H. W., and Roshko, A.: Elements of Gasdynamics. John Wiley & Sons, Inc., 1957.

17. Oswatitsch, Klaus, and Berndt, Sune B.: Aerodynamic Similarity at Axisymmetric Transonic Flow Around Slender Bodies. KTH-Aero TN 15, Roy. Inst. Tech., Division of Aeronautics, Stockholm, Sweden, 1950.

18. Staff of the Computing Section (under the direction of Zdenek Kopal): Tables of Supersonic Flow Around Cones. Tech. Rep. No. 1, Dept. Elect. Engr., Center of Analysis, M.I.T., 1947.

19. Laitone, E. V.: The Subsonic Axial Flow About a Body of Revolution. Quart. Appl. Math., vol. 5, no. 2, July 1947, pp. 227-231.

20. Berndt, Sune B.: Theoretical Aspects of the Calibration of Transonic Test Sections. Flygtekniska Forsoksanstalten Rep. 74, Stockholm, Sweden, 1957. (Supersedes FFA Rapp. AE-400)

21. Baldwin, Barrett S., Jr., Turner, John B., and Knechtel, Earl D.: Wall Interference in Wind Tunnels With Slotted and Porous Boundaries at Subsonic Speeds. NACA TN 3176, 1954. (Supersedes NACA RM A53E29)

TABLE I.- EXPERIMENTAL PRESSURE COEFFICIENTS ON SURFACE OF MODELS

Indicated Mach number	Orifice number[a]																
	1	2	3	4	5	6	7	8	9	10	11	12	13	14	15	16	17
(a) Circular cone-cylinder, 0.25-percent blockage; $\alpha = 0^\circ$																	
0.601	0.090	0.076	0.067	0.058	0.049	0.038	0.024	0.005	-0.034	-0.078	-0.259	-0.095	-0.063	-0.035	-0.016	0.058	0.025
.701	.096	.082	.071	.063	.054	.043	.028	.008	-.032	-.079	-.283	-.113	-.068	-.036	-.016	.061	.028
.800	.100	.086	.076	.068	.058	.047	.032	.012	-.030	-.080	-.309	-.123	-.068	-.037	-.016	.067	.033
.850	.104	.091	.080	.072	.062	.051	.036	.015	-.025	-.072	-.282	-.242	-.058	-.037	-.017	.070	.036
.901	.109	.096	.086	.077	.068	.058	.043	.025	-.012	-.049	-.224	-.481	-.036	-.022	-.014	.073	.044
.920	.113	.100	.090	.082	.073	.063	.048	.031	-.001	-.034	-.196	-.484	-.262	.006	-.007	.080	.049
.939	.116	.104	.094	.086	.078	.068	.055	.040	.012	-.017	-.169	-.476	-.367	.042	.000	.084	.056
.960	.121	.109	.100	.092	.084	.076	.065	.051	.028	.001	-.140	-.450	-.352	-.210	.024	.090	.065
.981	.127	.114	.106	.098	.092	.085	.075	.064	.045	.023	-.110	-.412	-.326	-.223	.016	.098	.076
.989	.130	.117	.109	.102	.096	.089	.081	.072	.053	.032	-.098	-.398	-.314	-.213	-.067	.101	.081
1.001	.134	.121	.112	.104	.100	.094	.086	.079	.063	.044	-.082	-.380	-.298	-.202	-.088	.104	.087
1.011	.142	.130	.119	.111	.103	.098	.092	.086	.073	.057	-.072	-.361	-.282	-.189	-.087	.109	.092
1.020	.140	.134	.127	.117	.109	.099	.092	.089	.079	.065	-.056	-.347	-.270	-.180	-.083	.115	.094
1.031	.120	.120	.120	.120	.120	.115	.105	.094	.081	.067	-.042	-.336	-.264	-.179	-.080	.119	.106
1.040	.107	.112	.118	.121	.124	.126	.122	.113	.095	.081	-.026	-.318	-.244	-.161	-.075	.119	.122
1.050	.099	.102	.104	.103	.101	.104	.109	.117	.118	.108	-.002	-.297	-.220	-.131	-.059	.102	.110
1.062	.100	.100	.100	.100	.100	.103	.103	.101	.099	.094	-.002	-.287	-.216	-.126	-.040	.098	.104
1.080	.096	.104	.100	.098	.099	.099	.096	.098	.096	.093	.008	-.266	-.204	-.127	-.051	.095	.098
1.100	.092	.091	.094	.089	.093	.097	.099	.098	.095	.093	.022	-.248	-.192	-.119	-.054	.088	.100
1.151	.084	.085	.084	.085	.085	.086	.086	.089	.087	.087	.034	-.215	-.167	-.105	-.049	.084	.088
1.200	.079	.078	.079	.081	.080	.079	.080	.083	.081	.082	.039	-.190	-.149	-.097	-.046	.080	.082
1.299	.077	.078	.078	.078	.078	.072	.073	.080	.075	.073	.037	-.157	-.128	-.087	-.047	.078	.075
1.400	.074	.074	.072	.079	.072	.071	.071	.075	.072	.072	.045	-.129	-.108	-.076	-.042	.073	.075
(b) Circular cone-cylinder, 0.005-percent blockage; $\alpha = 0^\circ$																	
.600	.092	.077	.067	.058	.048	.038	.025	.004	-.034	-.078	-.247	-.200	-.058	-.035	-.017	.057	.022
.797	.100	.082	.073	.064	.054	.044	.030	.008	-.032	-.079	-.300	-.200	-.060	-.037	-.018	.066	.031
.899	.113	.097	.088	.078	.068	.058	.044	.025	-.011	-.048	-.217	-.460	-.033	-.018	-.010	.076	.043
.964	.130	.113	.103	.095	.087	.079	.067	.057	.030	.007	-.129	-.444	-.352	-.205	.011	.091	.066
.980	.136	.117	.108	.100	.093	.087	.077	.064	.042	.021	-.104	-.417	-.328	-.225	-.055	.100	.076
.991	.141	.123	.113	.107	.102	.093	.083	.074	.052	.030	-.091	-.398	-.312	-.213	-.082	.107	.084
1.001	.152	.136	.127	.121	.113	.107	.098	.088	.069	.049	-.072	-.379	-.296	-.198	-.077	.119	.097
1.008	.159	.145	.137	.131	.120	.116	.111	.100	.082	.062	-.059	-.363	-.280	-.182	-.066	.129	.109
1.020	.138	.130	.125	.124	.119	.115	.110	.103	.091	.074	-.043	-.344	-.263	-.168	-.062	.124	.111
1.032	.121	.118	.115	.116	.112	.112	.108	.104	.094	.080	-.033	-.328	-.251	-.160	-.062	.113	.107
1.041	.109	.107	.108	.110	.109	.111	.109	.108	.095	.089	-.023	-.312	-.237	-.148	-.058	.108	.108
1.050	.113	.111	.105	.105	.104	.106	.103	.100	.099	.089	-.015	-.302	-.228	-.144	-.059	.108	.103
1.064	.100	.099	.099	.100	.100	.102	.096	.097	.096	.094	-.001	-.286	-.213	-.130	-.049	.098	.101
1.078	.098	.096	.096	.096	.096	.096	.096	.096	.096	.094	.008	-.268	-.203	-.125	-.052	.094	.095
1.100	.098	.096	.095	.095	.094	.094	.093	.092	.091	.090	.016	-.251	-.192	-.120	-.053	.094	.092

[a] See figure 1 for location.

TABLE I.- EXPERIMENTAL PRESSURE COEFFICIENTS ON SURFACE OF MODELS - Continued

Indicated Mach number	Orifice number[a]														
	1	2	3	4	5	6	7	8	9	10	11	12	13	14	15
(c) Elliptic cone-cylinder, 0.25-percent blockage; $\alpha = 0^{\circ}$															
0.601	0.050	0.051	0.036	0.026	0.021	0.012	0.002	-0.013	-0.035	-0.056	-0.098	-0.055	-0.041	-0.026	-0.012
.702	.053	.054	.039	.030	.024	.013	.003	-.014	-.039	-.062	-.109	-.061	-.045	-.029	-.012
.802	.057	.057	.042	.033	.026	.015	.004	-.015	-.044	-.073	-.129	-.074	-.053	-.032	-.013
.901	.067	.063	.048	.040	.030	.018	.005	-.015	-.053	-.091	-.172	-.117	-.086	-.040	-.003
.921	.069	.067	.050	.043	.032	.022	.009	-.012	-.051	-.092	-.200	-.143	-.109	-.032	-.005
.940	.072	.070	.054	.046	.036	.025	.013	-.006	-.043	-.083	-.215	-.185	-.142	-.052	-.002
.960	.077	.076	.060	.053	.044	.034	.023	.006	-.027	-.063	-.194	-.213	-.195	-.135	.042
.981	.084	.084	.067	.061	.052	.044	.035	.021	-.007	-.040	-.164	-.189	-.194	-.180	-.047
.990	.086	.086	.070	.064	.055	.048	.040	.028	.001	-.030	-.152	-.177	-.184	-.187	-.109
1.001	.089	.090	.073	.068	.060	.053	.046	.035	.011	-.019	-.138	-.163	-.169	-.180	-.106
1.010	.095	.095	.077	.071	.062	.056	.050	.040	.018	-.011	-.126	-.151	-.159	-.191	-.105
1.023	.091	.104	.090	.084	.072	.061	.053	.044	.026	.011	-.109	-.133	-.140	-.154	-.095
1.042	.064	.089	.083	.088	.088	.088	.087	.077	.055	.030	-.096	-.109	-.117	-.137	-.097
1.062	.059	.078	.065	.066	.064	.065	.067	.064	.054	.038	-.070	-.083	-.087	-.097	-.047
1.082	.064	.084	.065	.065	.064	.062	.061	.059	.051	.037	-.057	-.075	-.080	-.094	-.061
1.100	.056	.071	.058	.057	.062	.060	.062	.060	.054	.042	-.050	-.066	-.069	-.081	-.063
1.151	.049	.068	.055	.053	.055	.050	.052	.052	.047	.038	-.035	-.051	-.052	-.058	-.068
1.201	.044	.057	.046	.046	.050	.046	.047	.045	.042	.034	-.026	-.038	-.039	-.048	-.064
1.299	.041	.052	.048	.048	.049	.038	.040	.038	.040	.031	-.020	-.033	-.034	-.038	-.049
1.401	.040	.049	.044	.044	.043	.040	.039	.039	.040	.034	-.007	-.019	-.020	-.024	-.032

Indicated Mach number	Orifice number[a]													
	16	17	18	19	20	21	22	23	24	25	26	27	28	30
0.601	0.032	0.026	0.032	0.035	0.003	-0.003	0.000	0.006	-0.034	-0.042	-0.038	-0.025	0.147	-0.010
.702	.034	.030	.036	.038	.003	-.002	.000	.007	-.036	-.044	-.036	-.017	.153	-.008
.802	.038	.034	.043	.042	.004	.000	.000	.009	-.043	-.048	-.036	-.009	.159	-.006
.901	.044	.043	.053	.051	.005	.007	.010	.016	-.053	-.051	-.034	.000	.167	.001
.921	.045	.046	.056	.054	.009	.010	.013	.019	-.051	-.048	-.029	.005	.171	.005
.940	.049	.050	.060	.057	.013	.015	.018	.023	-.043	-.040	-.021	.013	.178	.010
.960	.056	.056	.066	.064	.023	.024	.027	.033	-.026	-.023	-.005	.028	.191	.019
.981	.064	.065	.075	.072	.036	.037	.039	.045	-.006	-.003	.015	.048	.208	.033
.990	.067	.068	.078	.075	.041	.042	.045	.050	.007	.005	.023	.055	.216	.037
1.001	.071	.072	.082	.078	.047	.048	.050	.055	.011	.015	.032	.066	.224	.043
1.010	.074	.074	.084	.081	.051	.051	.054	.059	.018	.022	.040	.072	.230	.048
1.023	.087	.088	.098	.095	.053	.055	.057	.061	.027	.030	.048	.082	.238	.050
1.042	.091	.092	.102	.099	.085	.086	.088	.094	.050	.052	.069	.107	.256	.082
1.062	.069	.070	.081	.078	.068	.069	.071	.077	.052	.056	.073	.106	.260	.062
1.082	.067	.068	.078	.075	.062	.064	.066	.071	.050	.054	.072	.104	.258	.055
1.100	.059	.060	.071	.067	.062	.064	.067	.072	.051	.055	.072	.104	.255	.062
1.151	.055	.056	.067	.064	.053	.054	.057	.063	.046	.050	.069	.103	.242	.048
1.201	.049	.049	.061	.057	.047	.050	.052	.057	.042	.046	.068	.103	.233	.044
1.299	.050	.050	.063	.057	.041	.044	.048	.051	.038	.043	.067	.110	.234	.037
1.401	.044	.043	.056	.048	.042	.046	.048	.052	.039	.041	.066	.107	.217	.035

[a]See figure 1 for location.

TABLE I.- EXPERIMENTAL PRESSURE COEFFICIENTS ON SURFACE OF MODELS - Continued

Indicated Mach number	Orifice number[a]														
	1	2	3	4	5	6	7	8	9	10	11	12	13	14	15
(d) Elliptic cone-cylinder, 0.25-percent blockage; $\alpha = 0.26^{\circ}$															
0.599	0.045	0.047	0.032	0.023	0.018	0.009	0.000	-0.016	-0.038	-0.058	-0.098	-0.056	-0.023	-0.028	-0.012
.800	.054	.055	.040	.031	.025	.015	.002	-.017	-.044	-.074	-.128	-.074	-.035	-.031	-.013
.900	.062	.060	.044	.037	.027	.016	.003	-.018	-.055	-.094	-.178	-.117	-.077	-.040	-.006
.939	.068	.066	.050	.043	.033	.022	.010	-.009	-.045	-.084	-.218	-.190	-.141	-.051	-.001
.980	.078	.078	.061	.055	.046	.038	.030	.016	-.013	-.045	-.170	-.195	-.197	-.179	.003
.992	.082	.082	.065	.061	.052	.044	.037	.025	.000	-.031	-.132	-.178	-.181	-.189	-.108
1.001	.084	.085	.068	.063	.054	.048	.041	.029	.006	-.024	-.143	-.168	-.172	-.184	-.108
1.011	.092	.093	.073	.068	.059	.052	.047	.038	.016	-.012	-.126	-.152	-.156	-.173	-.104
1.020	.095	.101	.083	.075	.061	.054	.050	.042	.023	-.003	-.115	-.140	-.145	-.162	-.099
1.041	.063	.087	.079	.084	.082	.082	.079	.069	.048	.024	-.098	-.114	-.104	-.143	-.100
1.060	.056	.073	.058	.060	.059	.060	.062	.058	.046	.028	-.076	-.090	-.078	-.103	-.046
1.102	.049	.065	.051	.054	.057	.055	.056	.055	.049	.036	-.053	-.068	-.059	-.086	-.061
1.200	.034	.052	.041	.040	.044	.040	.041	.040	.038	.032	-.029	-.041	-.032	-.051	-.064
1.400	.039	.045	.043	.041	.040	.038	.038	.038	.041	.042	-.009	-.022	-.019	-.029	-.036

Indicated Mach number	Orifice number[a]													
	16	17	18	19	20	21	22	23	24	25	26	27	28	30
0.599	0.028	0.022	0.025	0.024	0.000	-0.007	-0.006	-0.003	-0.037	-0.045	-0.041	-0.035	0.172	-0.006
.800	.034	.029	.035	.031	.002	-.004	-.002	.000	-.045	-.051	-.043	-.026	.186	-.001
.900	.039	.039	.046	.041	.002	.003	.005	.007	-.055	-.055	-.039	-.016	.190	.005
.939	.046	.046	.053	.048	.011	.011	.013	.015	-.045	-.042	-.026	-.002	.202	.015
.980	.058	.058	.066	.061	.030	.030	.032	.034	-.013	-.008	.006	.029	.229	.035
.992	.063	.063	.070	.065	.038	.038	.040	.042	.000	.003	.018	.041	.240	.042
1.001	.065	.066	.073	.068	.042	.042	.044	.046	.006	.009	.024	.047	.244	.046
1.011	.070	.071	.078	.073	.047	.048	.049	.051	.017	.020	.034	.057	.254	.052
1.020	.077	.077	.085	.079	.050	.050	.052	.054	.024	.027	.041	.068	.260	.055
1.041	.096	.086	.094	.089	.078	.079	.081	.083	.044	.047	.060	.087	.274	.084
1.060	.062	.063	.071	.065	.063	.064	.066	.068	.044	.047	.061	.088	.276	.066
1.102	.056	.056	.063	.056	.057	.059	.061	.064	.047	.049	.064	.090	.278	.065
1.200	.043	.043	.051	.046	.042	.044	.046	.048	.037	.042	.059	.089	.262	.048
1.400	.043	.040	.050	.042	.039	.043	.045	.046	.038	.039	.060	.095	.252	.042

[a] See figure 1 for location.

TABLE I.- EXPERIMENTAL PRESSURE COEFFICIENTS ON SURFACE OF MODELS - Continued

Indicated Mach number	Orifice number[a]														
	1	2	3	4	5	6	7	8	9	10	11	12	13	14	15
(e) Elliptic cone-cylinder, 0.25-percent blockage; $\alpha = -0.26^{\circ}$															
0.599	0.057	0.057	0.042	0.032	0.027	0.017	0.006	-0.010	-0.032	-0.053	-0.094	-0.053	-0.022	-0.024	-0.010
.798	.063	.061	.046	.038	.030	.020	.007	-.011	-.041	-.068	-.124	-.072	-.035	-.030	-.010
.899	.072	.069	.053	.045	.035	.024	.009	-.012	-.049	-.087	-.162	-.113	-.079	-.041	-.002
.938	.079	.076	.060	.053	.042	.031	.018	-.002	-.039	-.080	-.210	-.178	-.135	-.050	.000
.982	.089	.088	.072	.067	.057	.048	.039	.024	-.004	-.037	-.162	-.186	-.188	-.175	-.046
.990	.091	.091	.075	.069	.061	.053	.044	.031	.004	-.027	-.149	-.174	-.178	-.182	-.104
1.000	.096	.096	.079	.074	.065	.058	.051	.039	.014	-.016	-.134	-.159	-.163	-.177	-.104
1.012	.101	.101	.082	.076	.067	.061	.055	.044	.021	-.008	-.123	-.148	-.152	-.167	-.103
1.023	.095	.109	.095	.091	.077	.066	.058	.048	.031	.005	-.105	-.129	-.130	-.149	-.093
1.042	.070	.096	.088	.092	.091	.091	.088	.078	.056	.031	-.095	-.108	-.096	-.136	-.098
1.061	.067	.080	.067	.071	.070	.071	.068	.065	.057	.040	-.070	-.081	-.066	-.093	-.048
1.099	.058	.074	.062	.065	.065	.062	.065	.062	.058	.046	-.049	-.062	-.050	-.079	-.063
1.201	.050	.062	.051	.050	.057	.050	.051	.049	.047	.041	-.022	-.034	-.024	-.044	-.062
1.400	.043	.052	.048	.047	.046	.044	.044	.044	.044	.039	-.004	-.016	-.011	-.019	-.028

Indicated Mach number	Orifice number[a]														
	16	17	18	19	20	21	22	23	24	25	26	27	28	29	30
0.599	0.036	0.033	0.038	0.046	0.006	0.001	0.006	0.016	-0.032	-0.038	-0.033	-0.019	0.136	-0.011	
.798	.041	.040	.047	.052	.007	.005	.010	-.005	-.041	-.044	-.032	-.006	.146	-.009	
.899	.048	.049	.057	.061	.010	.012	.016	.026	-.050	-.046	-.030	-.003	.153	-.002	
.938	.056	.057	.065	.069	.019	.021	.024	.035	-.038	-.035	-.017	.017	.166	.006	
.982	.069	.070	.079	.082	.040	.042	.045	.055	-.003	.000	.019	.051	.197	.028	
.990	.072	.073	.082	.086	.045	.047	.050	.060	.005	.008	.025	.059	.202	.032	
1.000	.077	.078	.086	.090	.052	.054	.057	.067	.015	.020	.036	.070	.210	.039	
1.012	.078	.080	.089	.093	.056	.057	.060	.070	.023	.026	.042	.076	.218	.042	
1.023	.093	.095	.104	.107	.058	.060	.063	.073	.030	.035	.052	.085	.224	.044	
1.042	.095	.096	.105	.108	.087	.088	.092	.101	.051	.054	.070	.102	.241	.074	
1.061	.073	.074	.083	.086	.069	.074	.078	.087	.054	.058	.074	.108	.247	.055	
1.099	.068	.071	.090	.093	.065	.066	.070	.078	.055	.058	.073	.106	.248	.053	
1.201	.053	.054	.064	.066	.052	.054	.057	.065	.047	.052	.071	.105	.229	.040	
1.400	.049	.048	.058	.057	.046	.050	.054	.062	.043	.045	.068	.107	.220	.031	

[a] See figure 1 for location.

TABLE I.- EXPERIMENTAL PRESSURE COEFFICIENTS ON SURFACE OF MODELS - Continued

Indicated Mach number	Orifice number[a]														
	1	2	3	4	5	6	7	8	9	10	11	12	13	14	15
(f) Elliptic cone-cylinder, 0.25-percent blockage; $\alpha = 0.53^\circ$															
0.603	0.040	0.041	0.028	0.018	0.013	0.005	-0.005	-0.019	-0.041	-0.060	-0.101	-0.059	-0.024	-0.028	-0.013
.801	.047	.050	.035	.025	.019	.009	-.002	-.021	-.050	-.077	-.132	-.076	-.037	-.032	-.015
.901	.056	.055	.040	.032	.023	.013	.000	-.021	-.057	-.097	-.188	-.114	-.066	-.036	-.010
.939	.062	.061	.045	.038	.028	.019	.007	-.013	-.048	-.086	-.221	-.200	-.148	-.053	-.001
.982	.073	.074	.057	.052	.043	.036	.027	.014	-.013	-.044	-.169	-.192	-.194	-.189	-.049
.993	.075	.076	.061	.055	.046	.040	.032	.020	-.004	-.034	-.155	-.180	-.183	-.193	-.110
1.000	.079	.080	.064	.058	.050	.044	.038	.027	.004	-.025	-.144	-.169	-.172	-.187	-.108
1.013	.087	.088	.069	.063	.054	.048	.043	.033	.013	-.014	-.128	-.153	-.156	-.174	-.104
1.023	.086	.096	.078	.072	.058	.049	.043	.036	.019	-.006	-.116	-.140	-.144	-.162	-.099
1.042	.056	.079	.071	.076	.076	.079	.078	.069	.050	.025	-.097	-.112	-.102	-.142	-.097
1.062	.055	.071	.055	.057	.055	.053	.055	.054	.043	.025	-.077	-.094	-.084	-.109	-.046
1.101	.045	.060	.050	.052	.053	.049	.052	.050	.044	-.032	-.056	-.072	-.063	-.088	-.060
1.202	.033	.048	.037	.036	.040	.036	.036	.035	.033	.025	-.035	-.048	-.040	-.056	-.066
1.401	.031	.039	.034	.033	.032	.030	.030	.030	.031	.025	-.017	-.029	-.026	-.032	-.039

Indicated Mach number	Orifice number[a]													
	16	17	18	19	20	21	22	23	24	25	26	27	28	30
0.603	0.024	0.017	0.019	0.013	-0.003	-0.011	-0.011	-0.013	-0.040	-0.047	-0.047	-0.044	0.180	-0.002
.801	.029	.024	.027	.020	-.002	-.007	-.007	-.010	-.048	-.055	-.047	-.031	.189	.002
.901	.035	.033	.038	.029	.000	-.002	-.001	-.003	-.058	-.059	-.046	-.024	.192	.010
.939	.040	.040	.045	.036	.007	.007	.007	.004	-.048	-.046	-.032	-.010	.205	.019
.982	.054	.054	.059	.051	.027	.027	.028	.025	-.013	-.010	.003	.025	.233	.041
.993	.057	.057	.063	.054	.032	.032	.034	.031	-.004	-.001	.012	.033	.241	.046
1.000	.061	.061	.067	.057	.038	.038	.038	.035	.004	.006	.020	.041	.248	.051
1.013	.066	.066	.070	.062	.043	.043	.044	.041	.013	.016	.029	.051	.256	.056
1.023	.074	.074	.079	.068	.043	.044	.044	.039	.019	.022	.035	.057	.263	.058
1.042	.080	.079	.085	.076	.078	.078	.078	.076	.045	.046	.058	.080	.282	.091
1.062	.059	.059	.065	.055	.055	.055	.056	.054	.042	.045	.058	.080	.285	.069
1.101	.054	.054	.060	.051	.052	.052	.053	.049	.042	.044	.057	.078	.286	.068
1.202	---	.038	.045	.035	.037	.038	.039	.036	.033	.036	.053	.077	.268	.051
1.401	.035	.033	.039	.028	.032	.035	.035	.033	.029	.031	.051	.081	.251	.041

[a] See figure 1 for location.

TABLE I.- EXPERIMENTAL PRESSURE COEFFICIENTS ON SURFACE OF MODELS - Continued

Indicated Mach number	Orifice number[a]														
	1	2	3	4	5	6	7	8	9	10	11	12	13	14	15
(g) Elliptic cone-cylinder, 0.25-percent blockage; $\alpha = -0.53^\circ$															
0.603	0.061	0.060	0.045	0.036	0.029	0.019	0.008	-0.009	-0.031	-0.051	-0.092	-0.051	-0.020	-0.024	-0.009
.802	.069	.066	.051	.042	.033	.022	.009	-.010	-.039	-.067	-.123	-.073	-.037	-.030	-.010
.901	.076	.074	.058	.049	.038	.027	.013	-.008	-.046	-.085	-.163	-.113	-.078	-.040	-.003
.940	.082	.080	.064	.057	.046	.035	.022	.002	-.036	-.077	-.209	-.178	-.135	-.046	-.002
.982	.092	.092	.075	.069	.060	.052	.043	.027	-.002	-.037	-.163	-.186	-.186	-.175	-.024
.992	.096	.096	.080	.075	.066	.058	.050	.036	.010	-.022	-.145	-.169	-.170	-.182	-.101
1.000	.098	.098	.082	.077	.068	.061	.053	.041	.016	-.015	-.135	-.160	-.162	-.176	-.102
1.014	.108	.108	.090	.083	.073	.067	.060	.050	.028	-.002	-.116	-.141	-.145	-.161	-.102
1.023	.104	.115	.101	.094	.081	.070	.062	.054	.036	.009	-.104	-.127	-.128	-.148	-.094
1.042	.080	.102	.093	.097	.096	.095	.093	.083	.062	.035	-.093	-.105	-.091	-.133	-.097
1.061	.071	.088	.074	.076	.075	.076	.076	.075	.069	.051	-.067	-.077	-.059	-.091	-.051
1.101	.054	.080	.069	.070	.071	.067	.070	.071	.066	.055	-.044	-.056	-.040	-.073	-.061
1.200	.054	.067	.055	.056	.058	.054	.055	.054	.052	.045	-.019	-.030	-.018	-.040	-.061
1.401	.048	.056	.052	.052	.051	.047	.046	.046	.047	.043	.000	-.012	-.005	-.016	-.024

Indicated Mach number	Orifice number[a]														
	16	17	18	19	20	21	22	23	24	25	26	27	28	30	
0.603	0.040	0.037	0.044	0.054	0.009	0.006	0.010	0.025	-0.030	-0.035	-0.031	-0.014	0.117	-0.015	
.802	.045	.045	.054	.063	.010	.010	.015	.029	-.040	-.041	-.028	.001	.125	-.012	
.901	.009	.053	.062	.071	.014	.016	.021	.035	-.047	-.043	-.027	.007	.129	-.007	
.940	.059	.061	.070	.078	.023	.025	.030	.044	-.035	-.031	-.014	.021	.142	.002	
.982	.072	.074	.083	.091	.043	.045	.050	.063	-.002	.003	.019	.053	.171	.022	
.992	.078	.080	.088	.096	.050	.052	.057	.071	.010	.015	.031	.066	.182	.029	
1.000	.080	.081	.090	.098	.054	.056	.061	.074	.016	.020	.037	.071	.188	.033	
1.014	.086	.088	.096	.104	.061	.064	.068	.091	.028	.033	.049	.082	.197	.040	
1.023	.097	.099	.108	.115	.064	.065	.070	.082	.036	.040	.056	.090	.204	.040	
1.042	.100	.102	.112	.119	.091	.093	.097	.110	.056	.059	.074	.107	.219	.072	
1.061	.079	.081	.090	.098	.076	.079	.084	.096	.063	.067	.082	.115	.227	.052	
1.101	.072	.075	.085	.092	.070	.072	.077	.090	.061	.064	.080	.112	.227	.051	
1.200	.057	.059	.069	.076	.056	.059	.063	.075	.052	.056	.076	.112	.206	.035	
1.401	.053	.052	.064	.066	.049	.054	.060	.070	.048	.050	.073	.114	.198	.027	

[a]See figure 1 for location.

TABLE I.- EXPERIMENTAL PRESSURE COEFFICIENTS ON SURFACE OF MODELS - Continued

Indicated Mach number	Orifice number[a]														
	1	2	3	4	5	6	7	8	9	10	11	12	13	14	15
(h) Elliptic cone-cylinder, 0.25-percent-blockage; $\alpha = 1.06^\circ$															
0.601	0.032	0.037	0.019	0.012	0.006	-0.001	-0.011	-0.025	-0.045	-0.065	-0.103	-0.060	-0.026	-0.030	-0.013
.802	.039	.042	.027	.017	.012	.002	-.010	-.027	-.055	-.082	-.134	-.078	-.040	-.034	-.015
.901	.047	.048	.033	.025	.017	.007	-.005	-.025	-.063	-.105	-.200	-.111	-.059	-.036	-.014
.940	.053	.054	.038	.033	.024	.015	.004	-.014	-.048	-.088	-.233	-.229	-.143	-.026	-.004
.980	.065	.065	.050	.045	.038	.031	.024	.011	-.015	-.045	-.176	-.195	-.188	-.204	-.001
.992	.067	.068	.052	.048	.041	.035	.029	.017	-.005	-.034	-.163	-.181	-.174	-.201	-.082
.998	.068	.070	.053	.050	.043	.038	.032	.021	.000	-.029	-.155	-.175	-.168	-.196	-.095
1.005	.075	.076	.058	.054	.046	.040	.036	.026	.007	-.019	-.142	-.161	-.156	-.185	-.097
1.022	.078	.088	.072	.065	.052	.043	.038	.032	.019	.006	-.124	-.143	-.137	-.167	-.092
1.039	.049	.075	.065	.072	.071	.073	.069	.055	.035	.011	-.106	-.125	-.127	-.154	-.102
1.060	.039	.059	.047	.050	.050	.048	.045	.045	.042	.026	-.078	-.094	-.082	-.109	-.065
1.102	.035	.050	.039	.042	.045	.041	.043	.043	.037	.025	-.063	-.079	-.071	-.096	-.060
1.198	.023	.039	.029	.029	.032	.028	.029	.028	.026	.020	-.042	-.054	-.046	-.063	-.069
1.384	.026	.033	.029	.027	.026	.025	.025	.024	.026	.020	-.022	-.033	-.029	-.038	-.047

Indicated Mach number	Orifice number[a]														
	16	17	18	19	20	21	22	23	24	25	26	27	28	30	
0.601	0.017	0.009	0.008	-0.007	-0.009	-0.016	-0.019	-0.029	-0.044	-0.052	-0.053	-0.059	0.171	0.006	
.802	.022	.016	.017	-.001	-.008	-.015	-.017	-.028	-.054	-.059	-.054	-.049	.178	.011	
.901	.029	.024	.026	.008	-.005	-.010	-.012	-.022	-.063	-.065	-.054	-.043	.182	.018	
.940	.035	.032	.034	.015	.002	.000	-.002	-.013	-.048	-.048	-.037	-.030	.194	.029	
.980	.047	.046	.049	.031	.022	.021	.019	.008	-.016	-.015	-.003	.006	.223	.051	
.992	.050	.049	.051	.033	.027	.026	.024	.013	-.006	-.006	.005	.017	.230	.057	
.998	.052	.051	.053	.035	.030	.029	.027	.015	-.003	-.001	.010	.021	.233	.059	
1.005	.056	.055	.057	.039	.034	.034	.032	.019	.005	.006	.018	.030	.242	.064	
1.022	.067	.066	.068	.051	.036	.035	.033	.020	.017	.018	.029	.039	.251	.068	
1.039	.073	.073	.075	.057	.068	.067	.064	.053	.032	.033	.043	.054	.264	.095	
1.060	.052	.051	.054	.036	.044	.044	.042	.031	.040	.041	.052	.064	.275	.077	
1.102	.044	.042	.045	.025	.043	.045	.043	.032	.035	.036	.047	.058	.268	.079	
1.198	.031	.030	.033	.016	.029	.029	.027	.017	.025	.027	.041	.056	.254	.061	
1.384	.030	.027	.031	.013	.026	.027	.025	.016	.024	.024	.044	.065	.251	.053	

[a] See figure 1 for location.

TABLE I.- EXPERIMENTAL PRESSURE COEFFICIENTS ON SURFACE OF MODELS - Continued

Indicated Mach number	Orifice number[a]														
	1	2	3	4	5	6	7	8	9	10	11	12	13	14	15
(i) Elliptic cone-cylinder 0.25-percent blockage; $\alpha = -1.06^\circ$															
0.599	0.071	0.065	0.052	0.043	0.034	0.023	0.012	-0.005	-0.028	-0.048	-0.087	-0.053	-0.028	-0.024	-0.008
.802	.080	.075	.058	.051	.040	.029	.016	-.004	-.034	-.061	-.117	-.071	-.036	-.029	-.007
.901	.091	.084	.070	.061	.050	.038	.022	.000	-.036	-.076	-.152	-.106	-.074	-.039	.000
.939	.094	.091	.074	.066	.055	.043	.027	.008	-.031	-.073	-.198	-.158	-.120	-.039	-.002
.979	.103	.102	.086	.079	.069	.061	.050	.035	.004	-.032	-.158	-.182	-.182	-.166	-.030
.988	.106	.105	.089	.083	.073	.065	.056	.041	.012	-.022	-.146	-.170	-.171	-.174	-.092
1.001	.114	.113	.095	.091	.081	.074	.066	.054	.027	-.005	-.123	-.148	-.150	-.164	-.099
1.009	.117	.117	.098	.092	.083	.076	.069	.057	.033	.002	-.115	-.140	-.142	-.156	-.099
1.022	.131	.126	.108	.099	.086	.078	.072	.063	.041	.012	-.101	-.126	-.129	-.145	-.094
1.039	.090	.109	.102	.106	.105	.105	.105	.094	.072	.044	-.088	-.099	-.084	-.125	-.095
1.060	.082	.097	.086	.087	.085	.085	.084	.084	.077	.058	-.063	-.071	-.051	-.084	-.054
1.102	.073	.087	.079	.083	.082	.077	.081	.080	.077	.063	-.042	-.052	-.034	-.067	-.062
1.198	.061	.076	.065	.065	.067	.062	.063	.063	.063	.058	-.011	-.022	-.008	-.033	-.060
1.397	.057	.066	.062	.061	.060	.057	.058	.057	.059	.053	.010	-.002	.010	-.005	-.015

Indicated Mach number	Orifice number[a]														
	16	17	18	19	20	21	22	23	24	25	26	27	28	30	
0.599	0.046	0.047	0.056	0.074	0.012	0.014	0.022	0.042	-0.028	-0.028	-0.022	0.000	0.065	-0.020	
.802	.053	.056	.053	.083	.016	.018	.026	.047	-.036	-.033	-.019	.014	.069	-.019	
.901	.073	.065	.077	.093	.023	.028	.035	.057	-.038	-.033	-.014	.023	.080	-.013	
.939	.069	.071	.082	.097	.030	.034	.041	.062	-.030	-.025	-.005	.037	.089	-.006	
.979	.083	.085	.096	.111	.052	.054	.061	.082	.005	.010	.029	.069	.119	.015	
.988	.086	.089	.100	.114	.057	.060	.067	.086	.013	.018	.037	.077	.127	.019	
1.001	.094	.095	.106	.122	.067	.070	.077	.097	.029	.033	.053	.093	.141	.029	
1.009	.095	.097	.107	.124	.070	.073	.080	.099	.033	.039	.058	.098	.143	.031	
1.022	.102	.105	.116	.130	.073	.076	.082	.102	.042	.047	.067	.107	.151	.032	
1.039	.109	.112	.113	.137	.102	.105	.111	.131	.067	.070	.088	.126	.171	.067	
1.060	.090	.093	.104	.118	.084	.088	.094	.114	.072	.076	.095	.134	.174	.042	
1.102	.087	.090	.101	.116	.080	.083	.089	.108	.070	.073	.091	.130	.169	.040	
1.198	.068	.070	.081	.093	.065	.068	.074	.092	.061	.065	.086	.125	.149	.026	
1.397	.062	.063	.074	.084	.060	.065	.071	.089	.057	.061	.084	.126	.148	.021	

[a]See figure 1 for location.

TABLE I.- EXPERIMENTAL PRESSURE COEFFICIENTS ON SURFACE OF MODELS - Continued

Indicated Mach number	Orifice number[a]														
	1	2	3	4	5	6	7	8	9	10	11	12	13	14	15
(j) Elliptic cone-cylinder, 0.25-percent blockage; $\alpha = 2.12^{\circ}$															
0.600	0.012	0.012	0.000	-0.008	-0.012	-0.018	-0.026	-0.039	-0.057	-0.075	-0.113	-0.069	-0.035	-0.037	-0.020
.799	.023	.022	.007	-.002	-.008	-.016	-.025	-.042	-.067	-.092	-.140	-.085	-.046	-.040	-.019
.900	.029	.032	.015	.029	.000	-.010	-.022	-.042	-.079	-.118	-.200	-.109	-.058	-.043	-.020
.941	.033	.039	.022	.014	.007	-.003	-.013	-.031	-.065	-.106	-.253	-.244	-.127	-.026	-.013
.979	.043	.047	.033	.030	.023	.015	.007	-.005	-.030	-.062	-.197	-.207	-.193	-.230	.016
.989	.047	.051	.037	.034	.026	.020	.013	.001	-.021	-.052	-.185	-.195	-.182	-.222	-.017
1.000	.050	.055	.039	.038	.031	.022	.018	.007	-.013	-.043	-.173	-.182	-.170	-.210	-.078
1.014	.058	.059	.044	.042	.033	.028	.023	.014	-.004	-.031	-.157	-.167	-.155	-.195	-.090
1.020	.062	.070	.052	.048	.034	.028	.027	.020	.004	-.023	-.146	-.156	-.145	-.164	-.088
1.040	.037	.061	.049	.060	.057	.059	.055	.038	.018	-.008	-.126	-.137	-.125	-.168	-.104
1.060	.026	.047	.034	.042	.042	.039	.037	.033	.026	.010	-.100	-.107	-.091	-.122	-.053
1.098	.013	.039	.033	.035	.031	.031	.033	.028	.023	.012	-.086	-.094	-.078	-.106	-.057
1.202	.003	.025	.015	.016	.023	.017	.021	.018	.015	.011	-.060	-.066	-.052	-.075	-.068
1.403	.007	.016	.012	.014	.017	.017	.016	.015	.016	.011	-.036	-.044	-.032	-.049	-.056

Indicated Mach number	Orifice number[a]														
	16	17	18	19	20	21	22	23	24	25	26	27	28	30	
0.600	-0.002	-0.008	-0.009	-0.041	-0.027	-0.029	-0.035	-0.059	-0.059	-0.062	-0.067	-0.087	0.098	0.021	
.799	.006	-.003	-.001	-.034	-.026	-.028	-.034	-.059	-.068	-.071	-.068	-.078	.097	.028	
.900	.012	.007	.009	-.023	-.023	-.024	-.030	-.054	-.080	-.079	-.072	-.072	.101	.035	
.941	.021	.014	.018	-.007	-.007	-.016	-.021	-.045	-.065	-.065	-.058	-.056	.114	.046	
.979	.036	.029	.032	.002	.007	.004	-.001	-.023	-.031	-.030	-.024	-.023	.143	.067	
.989	.040	.033	.035	.006	.012	.009	.004	-.018	-.022	-.020	-.015	-.015	.150	.073	
1.000	.044	.037	.039	.010	.017	.014	.009	-.014	-.014	-.014	-.008	-.008	.157	.078	
1.014	.048	.042	.044	.016	.022	.020	.015	-.008	-.005	-.005	.001	.001	.163	.084	
1.020	.054	.048	.050	.021	.026	.024	.018	-.005	.003	.001	.008	.007	.170	.088	
1.040	.065	.060	.061	.032	.054	.052	.045	.022	.016	.016	.022	.022	.186	.091	
1.060	.046	.041	.053	.012	.036	.036	.031	.008	.026	.026	.032	.032	.197	.102	
1.098	.041	.037	.039	.009	.031	.029	.024	.000	.021	.020	.026	.025	.195	.096	
1.202	.022	.017	.019	-.014	.019	.019	.013	-.008	.015	.015	.025	.028	.185	.081	
1.403	.019	.014	.014	-.028	.013	.014	.009	-.009	.012	.011	.026	.031	.193	.069	

[a] See figure 1 for location.

TABLE I.- EXPERIMENTAL PRESSURE COEFFICIENTS ON SURFACE OF MODELS - Continued

Indicated Mach number	Orifice number [a]														
	1	2	3	4	5	6	7	8	9	10	11	12	13	14	15
(k) Elliptic cone-cylinder, 0.25-percent blockage; $\alpha = -2.12^{\circ}$															
0.602	0.094	0.085	0.069	0.060	0.048	0.037	0.023	0.006	-0.018	-0.038	-0.078	-0.047	-0.024	-0.020	-0.005
.802	.103	.097	.080	.070	.059	.047	.034	.014	-.018	-.047	-.107	-.058	-.020	-.020	-.005
.900	.111	.106	.088	.080	.070	.057	.040	.039	-.024	-.062	-.141	-.094	-.060	-.032	-.001
.940	.116	.112	.095	.086	.074	.063	.047	.037	-.016	-.059	-.188	-.146	-.102	-.036	.001
.981	.127	.125	.108	.101	.091	.081	.070	.052	.020	-.017	-.148	-.166	-.160	-.157	-.015
.991	.131	.129	.113	.105	.095	.087	.077	.061	.031	-.004	-.132	-.152	-.146	-.137	-.074
1.003	.134	.132	.115	.109	.099	.091	.082	.068	.040	.006	-.119	-.139	-.134	-.149	-.088
1.013	.142	.140	.121	.114	.104	.095	.088	.075	.049	.016	-.104	-.126	-.124	-.138	-.090
1.021	.145	.146	.127	.118	.106	.097	.091	.079	.055	.024	-.094	-.117	-.115	-.130	-.088
1.042	.107	.127	.121	.124	.123	.129	.129	.117	.091	.061	-.075	-.083	-.069	-.103	-.083
1.062	.104	.119	.107	.107	.104	.104	.110	.110	.096	.074	-.053	-.059	-.040	-.069	-.040
1.101	.096	.111	.098	.101	.101	.097	.105	.106	.099	.083	-.029	-.036	-.021	-.054	-.057
1.200	.085	.095	.085	.085	.087	.082	.085	.087	.087	.083	.005	-.006	.013	-.015	-.047
1.402	.077	.085	.079	.077	.079	.073	.073	.077	.078	.079	.026	.014	.031	.011	.001

Indicated Mach number	Orifice number [a]													
	16	17	18	19	20	21	22	23	24	25	26	27	28	30
0.602	0.063	0.068	0.079	0.110	0.025	0.029	0.025	0.024	-0.020	-0.017	-0.006	0.026	-0.107	-0.035
.802	.072	.078	.091	.120	.033	.038	.048	.081	-.022	-.017	.000	.044	-.103	-.035
.900	.083	.087	.101	.128	.041	.045	.056	.088	-.024	-.018	.003	.053	-.096	-.030
.940	.101	.094	.108	.135	.050	.054	.065	.096	-.151	-.009	.015	.065	-.078	-.022
.981	.105	.108	.122	.149	.072	.076	.086	.117	.021	.027	.050	.099	-.056	-.001
.991	.110	.113	.126	.153	.078	.083	.093	.124	.032	.038	.060	.110	-.051	.004
1.003	.112	.116	.129	.156	.083	.088	.097	.128	.041	.047	.069	.117	-.041	.009
1.013	.118	.121	.134	.160	.089	.094	.104	.134	.050	.056	.078	.126	-.040	.014
1.021	.122	.126	.139	.165	.092	.096	.106	.137	.056	.063	.085	.132	-.035	.014
1.042	.127	.131	.145	.171	.124	.125	.137	.168	.088	.092	.112	.159	-.004	.052
1.062	.110	.114	.128	.153	.107	.112	.112	.152	.091	.096	.117	.165	-.015	.026
1.101	.105	.109	.123	.149	.102	.106	.115	.145	.092	.096	.117	.164	-.019	.022
1.200	.088	.091	.106	.130	.085	.090	.100	.127	.083	.088	.111	.158	-.025	.010
1.402	.079	.082	.097	.117	.075	.082	.092	.118	.073	.081	.105	.155	.017	-.007

[a] See figure 1 for location.

TABLE I.- EXPERIMENTAL PRESSURE COEFFICIENTS ON SURFACE OF MODELS - Continued

Indicated Mach number	Orifice number[a]														
	1	2	3	4	5	6	7	8	9	10	11	12	13	14	15
(1) Elliptic cone-cylinder, 0.25-percent blockage; α = 4.24°															
0.602	-0.041	-0.033	-0.041	-0.047	-0.048	-0.050	-0.053	-0.063	-0.078	-0.096	-0.131	-0.086	-0.049	-0.049	-0.027
.800	-.031	-.026	-.037	-.043	-.048	-.052	-.058	-.072	-.094	-.117	-.165	-.104	-.062	-.053	-.029
.902	-.018	-.013	-.028	-.035	-.043	-.048	-.058	-.075	-.108	-.148	-.260	-.131	-.069	-.050	-.027
.942	-.009	-.004	-.020	-.026	-.036	-.040	-.049	-.064	-.091	-.126	-.269	-.276	-.226	-.021	-.015
.984	.003	.009	-.008	-.012	-.022	-.027	-.031	-.042	-.060	-.087	-.216	-.228	-.217	-.261	.024
.994	.005	.012	-.006	-.009	-.020	-.024	-.027	-.037	-.054	-.079	-.205	-.217	-.207	-.252	-.013
1.002	.011	.020	.001	-.001	-.014	-.019	-.021	-.028	-.044	-.067	-.190	-.202	-.190	-.235	-.094
1.012	.019	.027	.005	.002	-.013	-.015	-.018	-.026	-.038	-.059	-.179	-.190	-.179	-.224	-.101
1.022	.021	.037	.020	.016	-.002	-.011	-.018	-.025	-.034	-.050	-.161	-.170	-.159	-.200	-.093
1.041	-.002	.033	.017	.022	.020	.020	.024	-.008	-.017	-.038	-.152	-.164	-.154	-.198	-.120
1.060	-.013	.011	.000	.000	.002	.003	-.001	-.003	-.006	-.018	-.121	-.129	-.114	-.146	-.066
1.099	-.025	.007	-.001	-.007	-.009	-.007	-.005	-.007	-.010	-.019	-.111	-.118	-.104	-.133	-.068
1.203	-.028	-.012	-.016	-.017	-.014	-.016	-.016	-.017	-.017	-.021	-.087	-.096	-.081	-.103	-.085
1.401	-.027	-.017	-.018	-.022	-.018	-.017	-.020	-.017	-.020	-.023	-.065	-.076	-.062	-.078	-.084

Indicated Mach number	Orifice number[a]													
	16	17	18	19	20	21	22	23	24	25	26	27	28	30
0.602	-0.041	-0.044	-0.029	-0.328	-0.056	-0.058	-0.046	-0.293	-0.079	-0.081	-0.070	-0.281	-0.049	0.055
.800	-.039	-.041	-.028	-.319	-.060	-.063	-.051	-.301	-.094	-.096	-.077	-.289	-.057	.063
.902	-.029	-.033	-.022	-.303	-.059	-.061	-.047	-.297	-.108	-.108	-.077	-.290	-.051	.074
.942	-.021	-.025	-.015	-.290	-.050	-.053	-.040	-.287	-.091	-.092	-.061	-.273	-.034	.083
.984	-.007	-.011	-.003	-.272	-.033	-.035	-.027	-.269	-.060	-.062	-.033	-.245	-.008	.103
.994	-.004	-.008	.001	-.267	-.028	-.032	-.023	-.265	-.053	-.055	-.027	-.238	.002	.108
1.002	.004	.000	.007	-.260	-.022	-.025	-.018	-.260	-.044	-.045	-.016	-.229	.007	.117
1.012	.007	.004	.009	-.257	-.019	-.023	-.015	-.259	-.038	-.040	-.011	-.226	.010	.123
1.022	.021	.018	.023	-.231	-.020	-.023	-.018	-.249	-.032	-.036	-.011	-.220	.013	.125
1.041	.028	.025	.027	-.234	.023	.019	.026	-.214	-.016	-.018	.012	-.188	.040	.152
1.060	.005	.000	.000	-.248	-.001	-.005	.000	-.234	-.006	-.008	.018	-.196	.042	.148
1.099	-.001	-.006	-.007	-.221	-.007	-.012	-.015	-.233	-.011	-.015	.005	-.190	.043	.139
1.203	-.014	-.022	-.026	-.217	-.017	-.022	-.028	-.212	-.019	-.021	-.007	-.151	.040	.123
1.401	-.019	-.029	-.030	-.215	-.022	-.027	-.037	-.161	-.021	-.027	-.018	-.090	.078	.107

[a]See figure 1 for location.

TABLE I.- EXPERIMENTAL PRESSURE COEFFICIENTS ON SURFACE OF MODELS - Concluded

Indicated Mach number	Orifice number[a]														
	1	2	3	4	5	6	7	8	9	10	11	12	13	14	15
(m) Elliptic cone-cylinder, 0.25-percent blockage; $\alpha = -4.24^\circ$															
0.601	0.145	0.134	0.115	0.102	0.089	0.074	0.059	0.039	0.013	-0.010	-0.053	-0.021	0.003	0.001	0.008
.800	.153	.144	.125	.113	.100	.087	.071	.049	.015	-.016	-.079	-.029	-.007	-.003	.005
.902	.163	.154	.136	.125	.111	.097	.079	.054	.013	-.027	-.116	-.057	-.018	-.011	.004
.941	.169	.162	.144	.135	.119	.105	.087	.063	.019	-.026	-.163	-.092	-.041	-.015	.007
.980	.178	.172	.154	.144	.132	.121	.106	.086	.049	.009	-.137	-.141	-.117	-.113	.036
.993	.182	.177	.159	.150	.139	.128	.115	.097	.064	.025	-.120	-.125	-.100	-.109	-.046
.999	.185	.180	.163	.153	.142	.132	.119	.102	.071	.034	-.110	-.117	-.094	-.104	-.063
1.012	.193	.187	.168	.159	.147	.138	.126	.110	.079	.044	-.093	-.104	-.086	-.096	-.066
1.020	.197	.195	.173	.164	.151	.141	.130	.115	.087	.053	-.082	-.094	-.078	-.089	-.065
1.042	.165	.182	.176	.177	.177	.177	.166	.148	.117	.083	-.057	-.062	-.043	-.069	-.065
1.061	.156	.168	.157	.157	.155	.162	.163	.156	.137	.107	-.029	-.034	-.011	-.033	-.038
1.100	.143	.159	.145	.152	.148	.156	.157	.149	.138	.120	.001	-.010	.007	-.022	-.043
1.202	.125	.140	.131	.129	.130	.131	.138	.135	.130	.125	.042	.033	.049	.020	-.019
1.401	.118	.128	.119	.116	.117	.116	.122	.123	.118	.119	.062	.054	.070	.048	.035

Indicated Mach number	Orifice number[a]													
	16	17	18	19	20	21	22	23	24	25	26	27	28	30
0.601	0.107	0.113	0.131	0.174	0.061	0.068	0.086	0.132	0.012	0.017	0.032	0.079	-0.227	-0.065
.800	.118	.124	.142	.183	.071	.078	.095	.140	.012	.022	.039	.095	-.242	-.068
.902	.129	.135	.154	.194	.081	.088	.105	.150	.012	.022	.046	.105	-.252	-.067
.941	.137	.143	.161	.201	.090	.097	.113	.157	.019	.029	.055	.115	-.242	-.062
.980	.148	.155	.173	.211	.108	.115	.130	.174	.049	.059	.084	.143	-.221	-.043
.993	.154	.161	.178	.217	.117	.123	.139	.181	.063	.072	.098	.155	-.213	-.037
.999	.158	.164	.182	.220	.121	.128	.143	.186	.070	.079	.104	.162	-.210	-.034
1.012	.163	.169	.186	.224	.128	.134	.149	.191	.080	.089	.114	.172	-.206	-.030
1.020	.169	.174	.192	.230	.132	.138	.152	.194	.087	.097	.121	.179	-.205	-.035
1.042	.182	.188	.206	.244	.163	.168	.182	.224	.118	.125	.148	.204	-.166	.011
1.061	.162	.168	.186	.223	.160	.164	.178	.219	.141	.152	.168	.222	-.180	-.011
1.100	.157	.163	.182	.221	.152	.156	.169	.209	.142	.151	.167	.221	-.179	-.015
1.202	.134	.139	.158	.194	.133	.139	.152	.190	.133	.144	.162	.217	-.185	-.024
1.401	.120	.125	.143	.178	.118	.124	.138	.177	.123	.132	.152	.209	-.164	-.029

[a] See figure 1 for location.

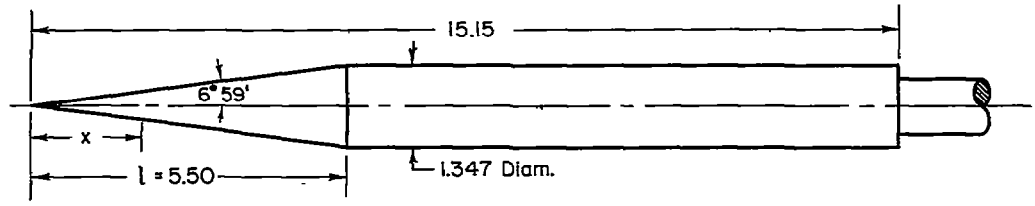

Table of orifice locations					
Orifice No.	x/l	6	.589	12	1.043
1	.082	7	.688	13	1.094
2	.183	8	.790	14	1.195
3	.285	9	.891	15	1.398
4	.385	10	.942	16 *	.385
5	.486	11	.994	17 *	.688

Circular cone-cylinder model

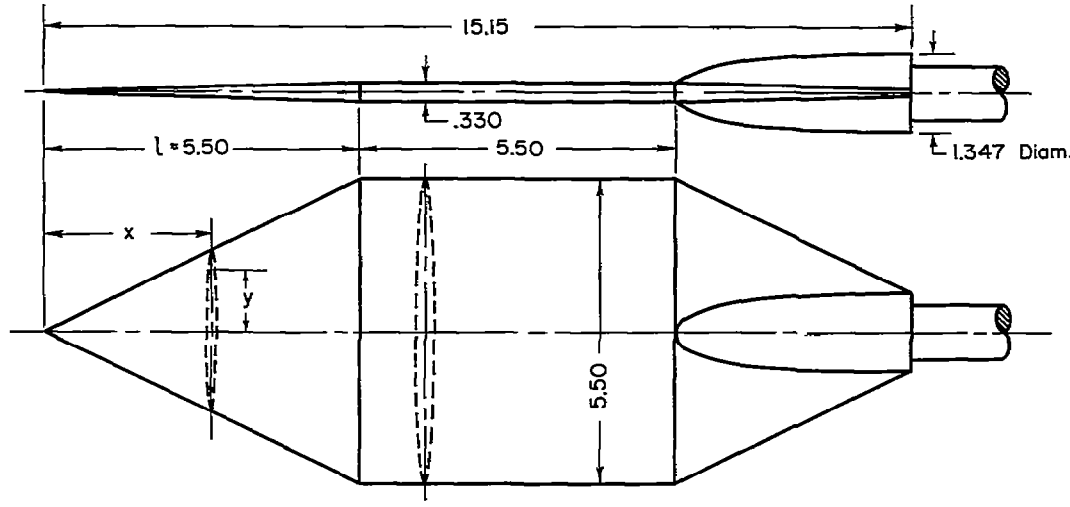

Table of orifice locations								
Orifice No.	x/l	y/mx	11	1.00	0	22	.70	.667
1	.10	0	12	1.05	0	23	.70	.889
2	.20	0	13	1.10	0	24	.90	.222
3	.30	0	14	1.20	0	25	.90	.444
4	.40	0	15	1.40	0	26	.90	.667
5	.50	0	16	.40	.222	27	.90	.889
6	.60	0	17	.40	.444	28	.90	1.000
7	.70	0	18	.40	.667	30*	.70	0
8	.80	0	19	.40	.889			
9	.90	0	20	.70	.222			
10	.95	0	21	.70	.444			

* Opposite surface

Elliptic cone-cylinder model

Figure 1.- Geometric details of models; dimensions in inches.

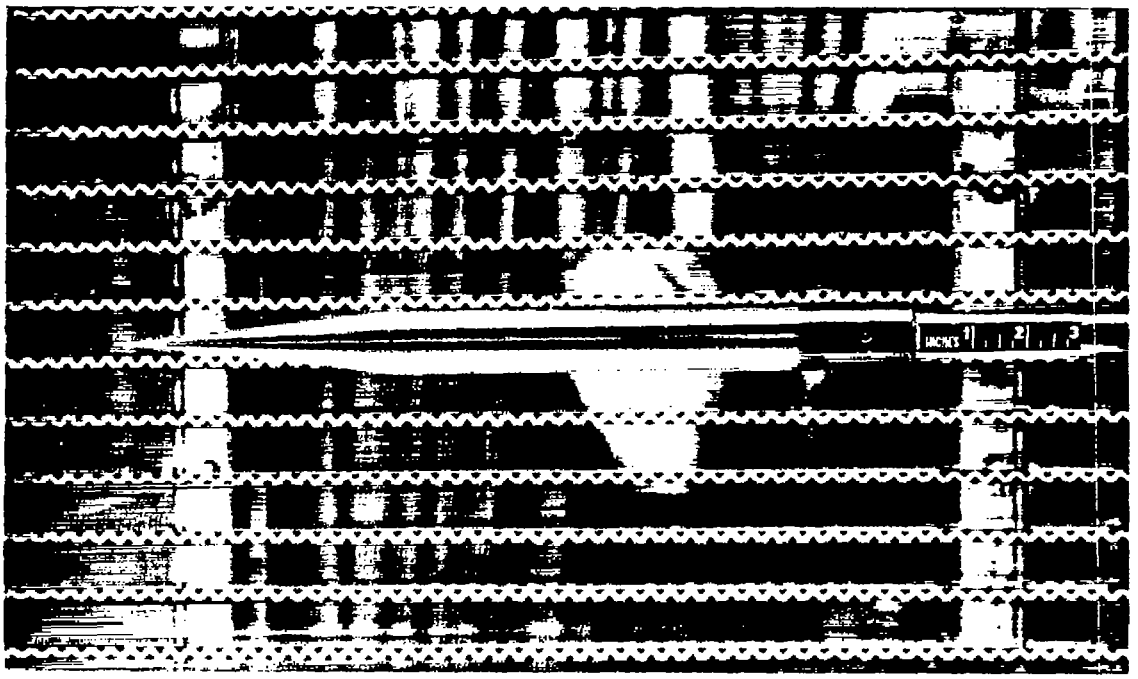

(a) Circular cone-cylinder model. A-22667

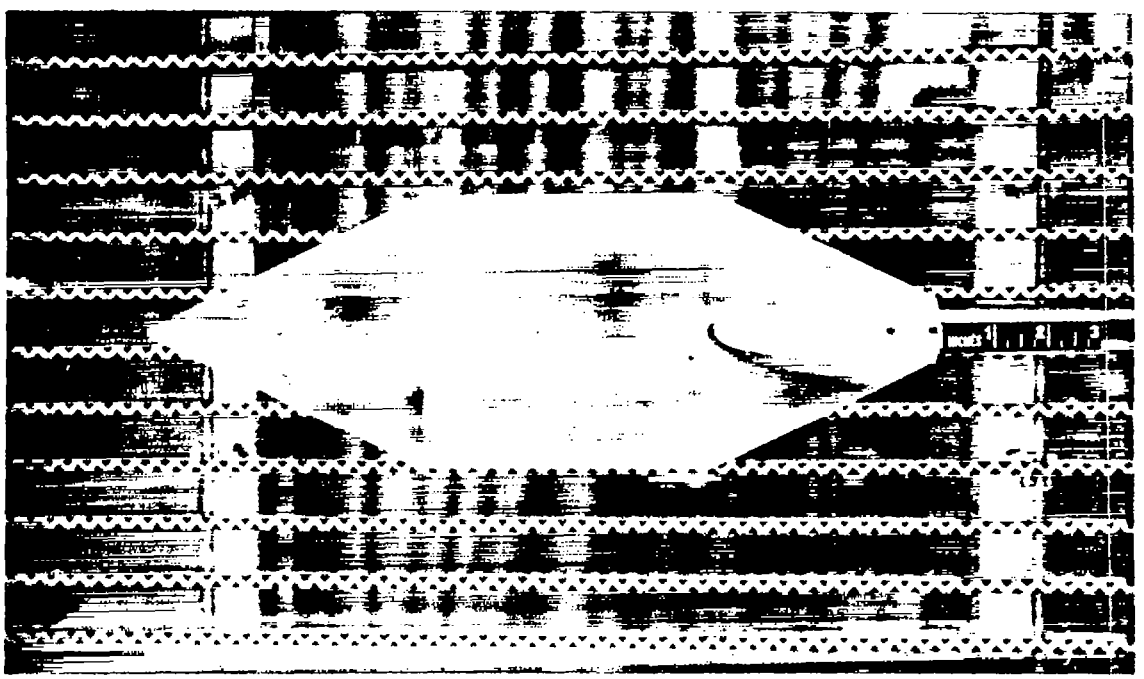

A-22668

(b) Elliptic cone-cylinder model.

Figure 2.- Photographs of models in the Ames 2- by 2-foot transonic wind tunnel.

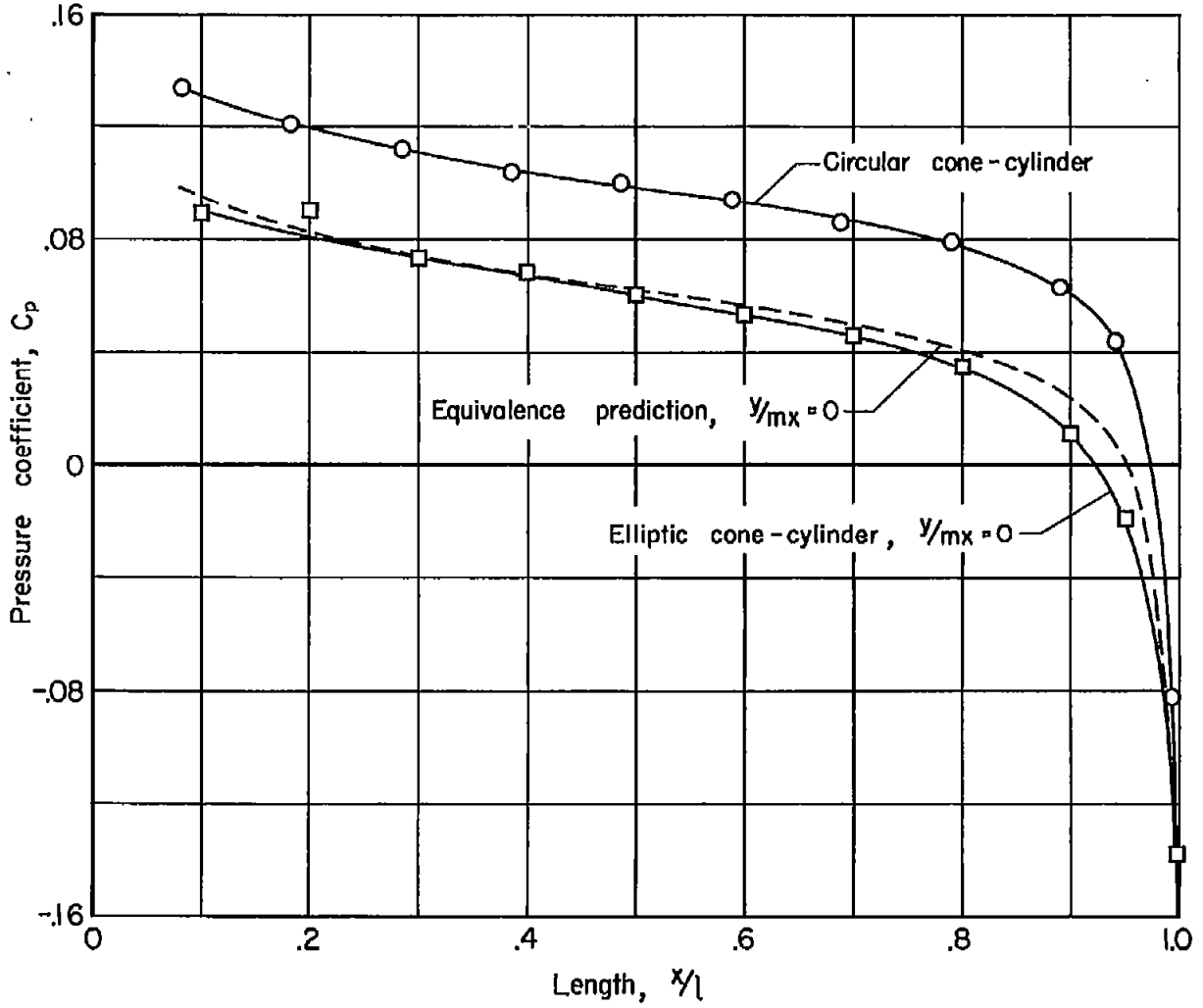

Figure 3.- Pressure distribution on circular cone-cylinder and along center line of elliptic cone-cylinder at a Mach number of 1 and at 0° angle of attack.

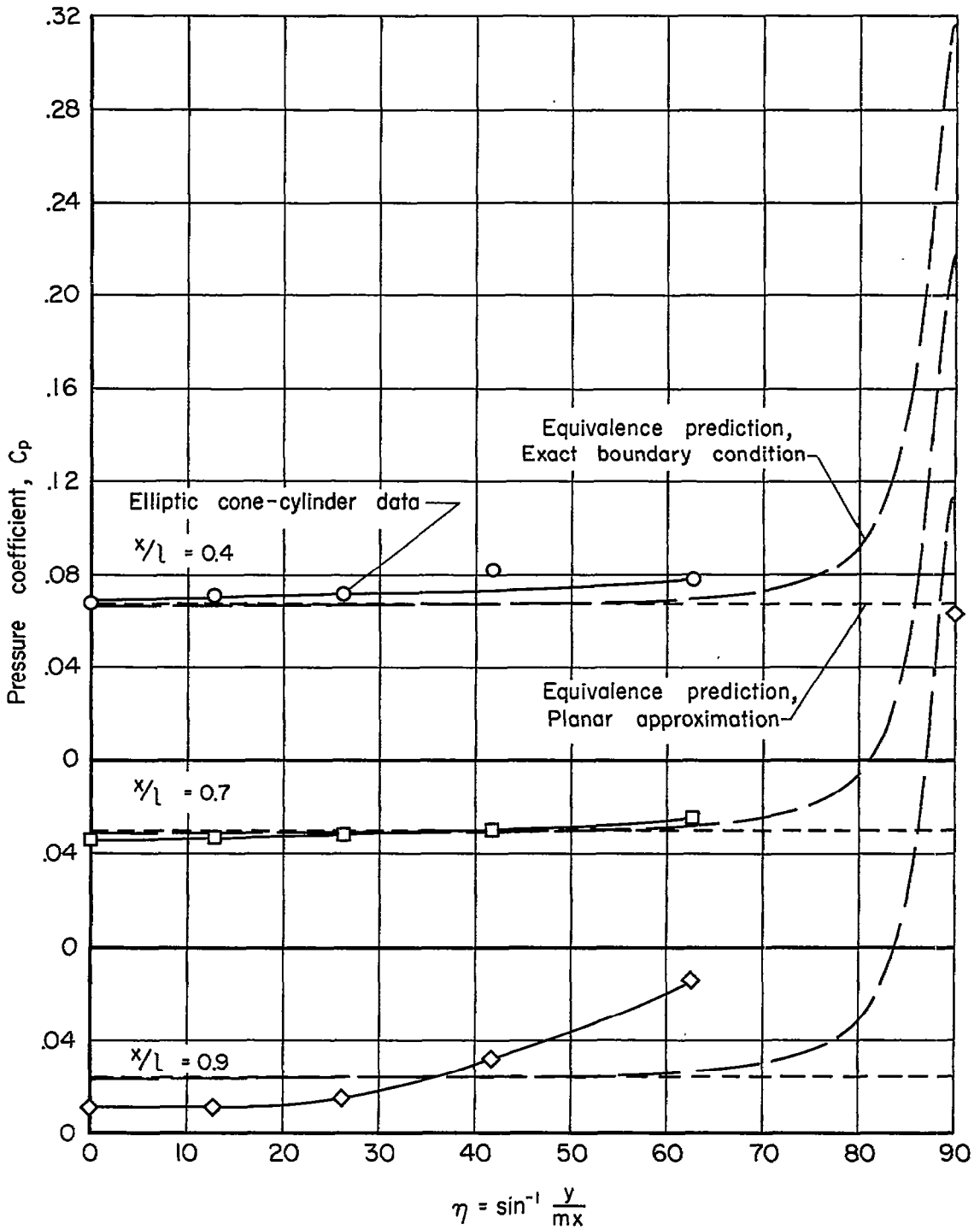

Figure 4.- Pressure distribution in spanwise direction on elliptic cone-cylinder at a Mach number of 1 and at 0° angle of attack.

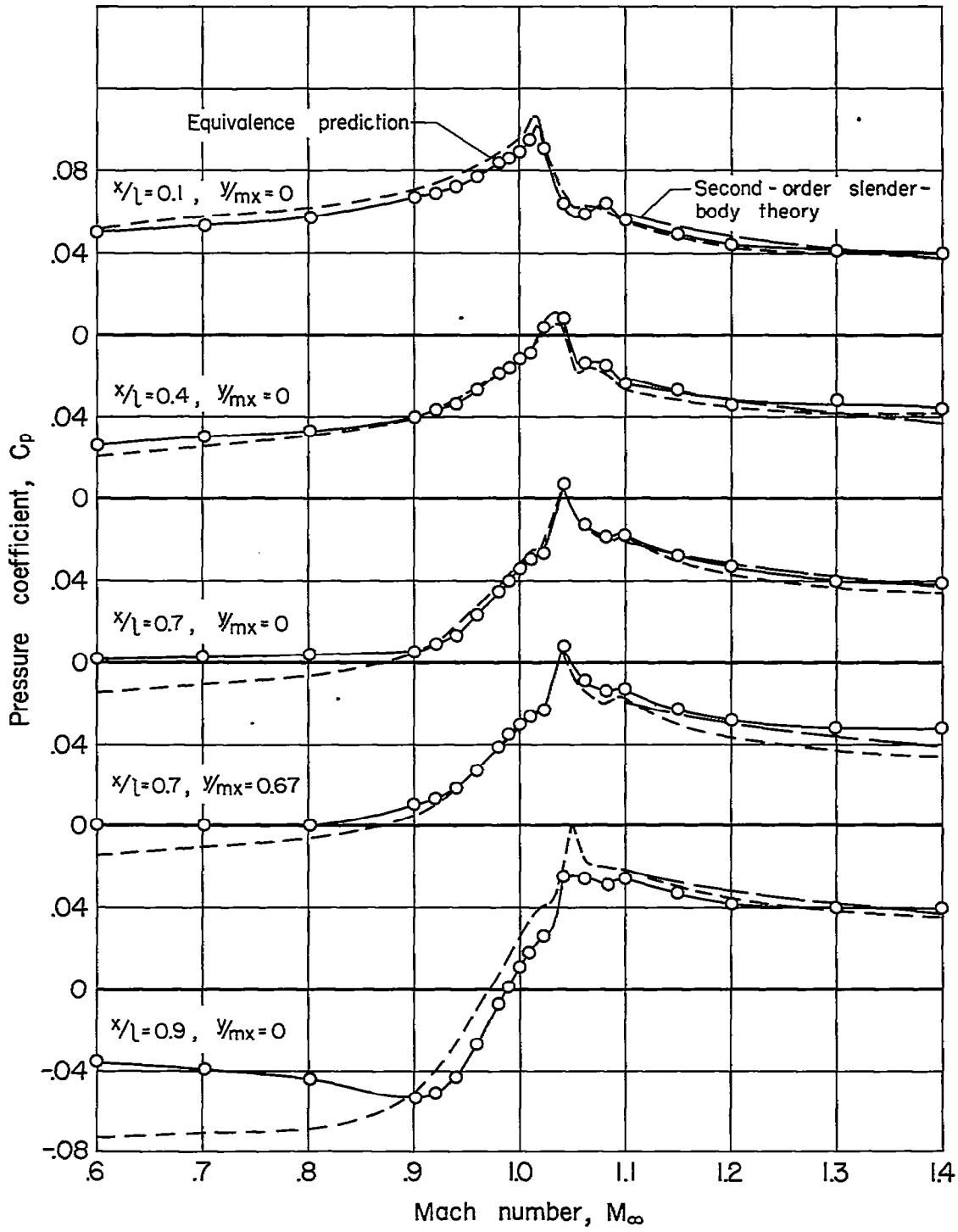

Figure 5.- Pressure coefficient at several locations on elliptic cone-cylinder as a function of Mach number at 0° angle of attack.

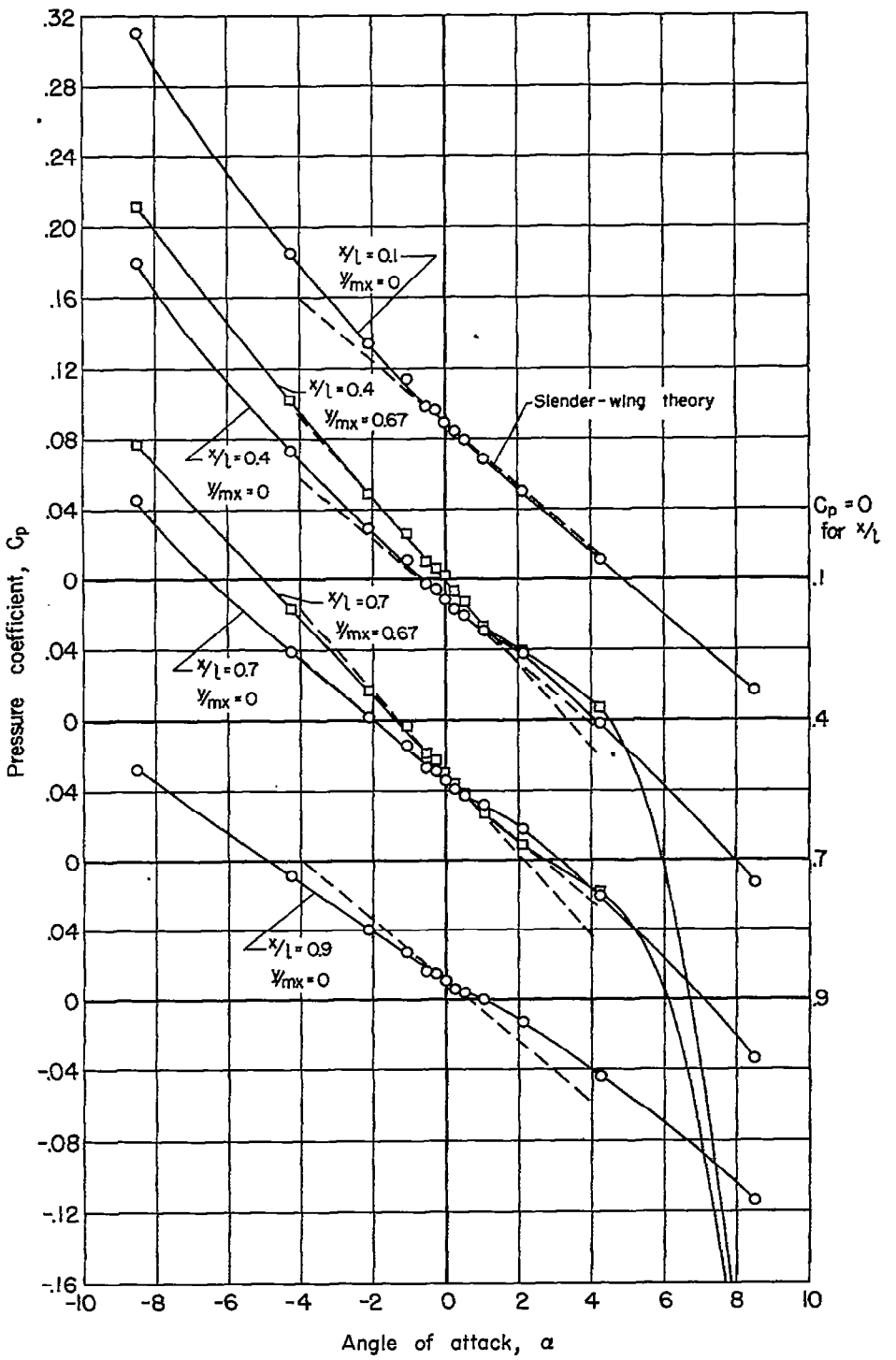

Figure 6.- Pressure coefficient at several locations on elliptic cone-cylinder as a function of angle of attack at a Mach number of 1.

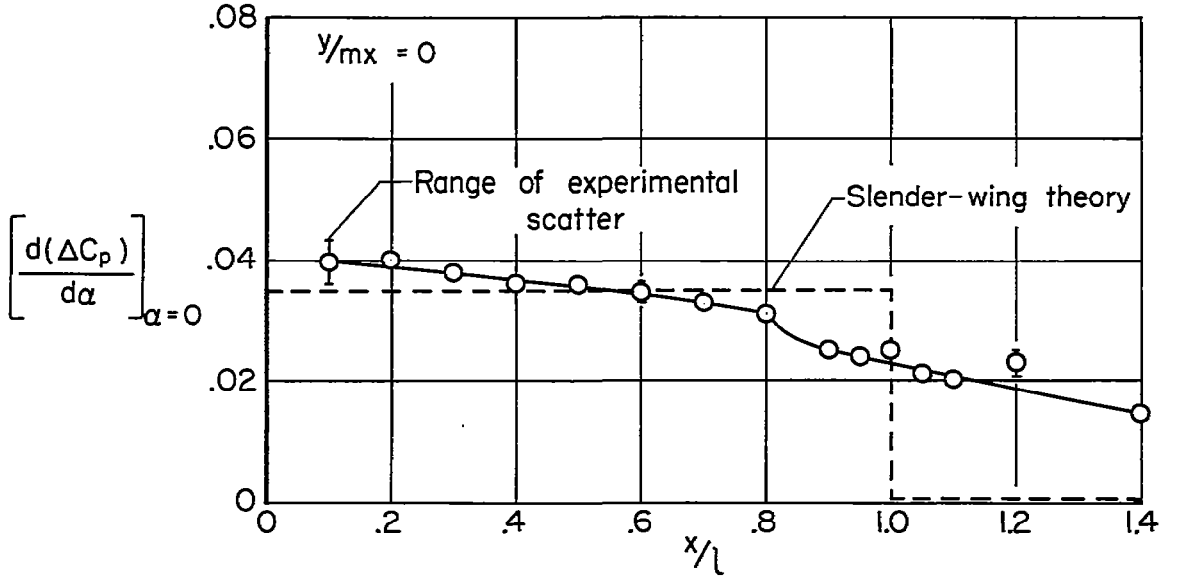

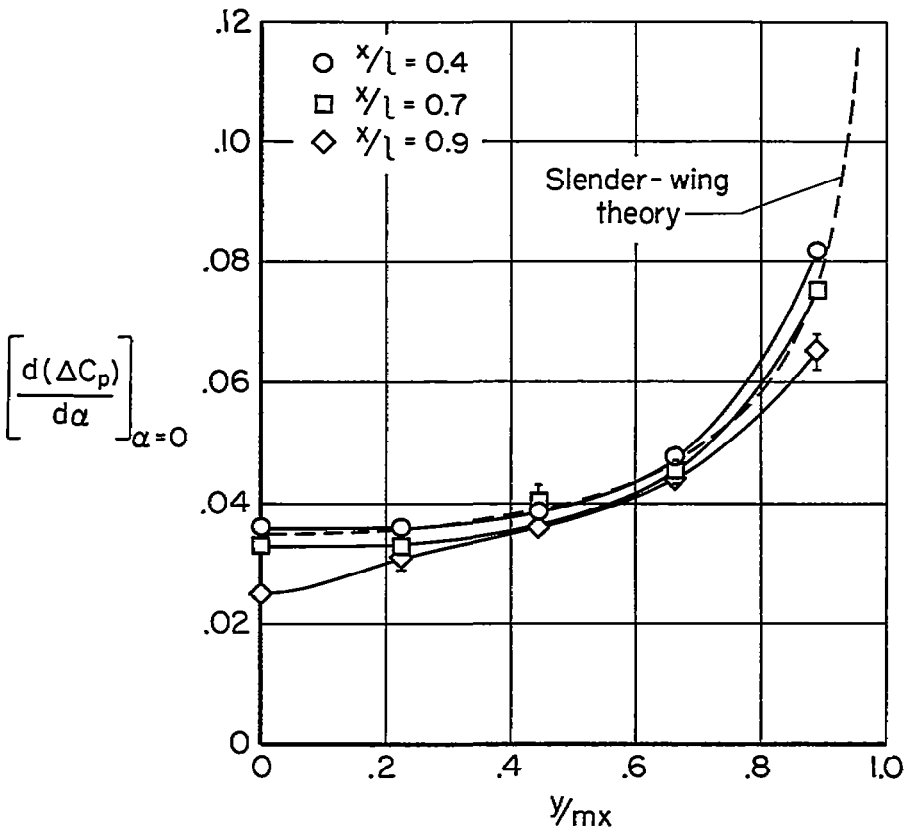

Figure 7.- The rate of change of aerodynamic loading with α on elliptic cone-cylinder at a Mach number of 1.

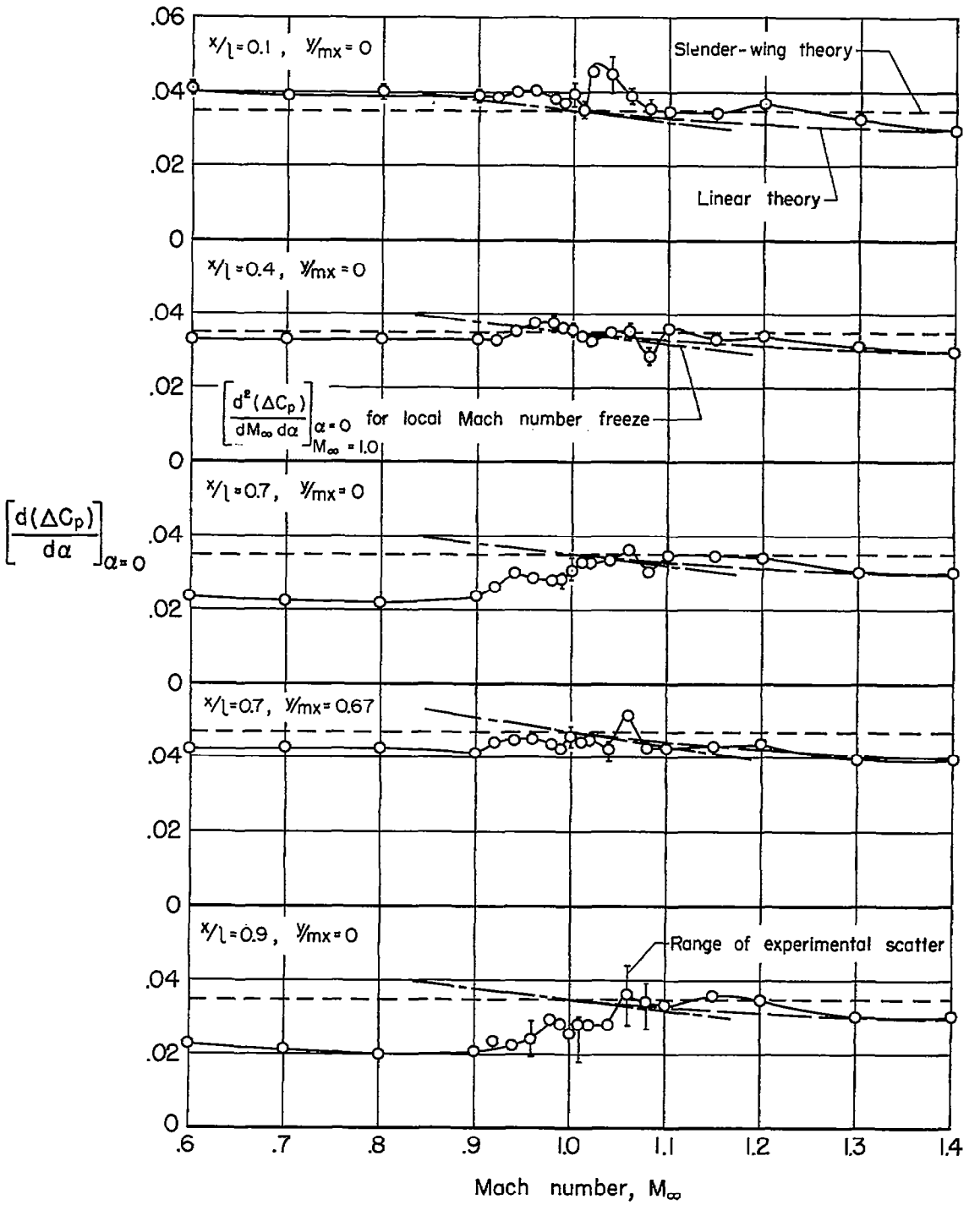

Figure 8.- The rate of change of aerodynamic loading with α at several locations on elliptic cone-cylinder as a function of Mach number.

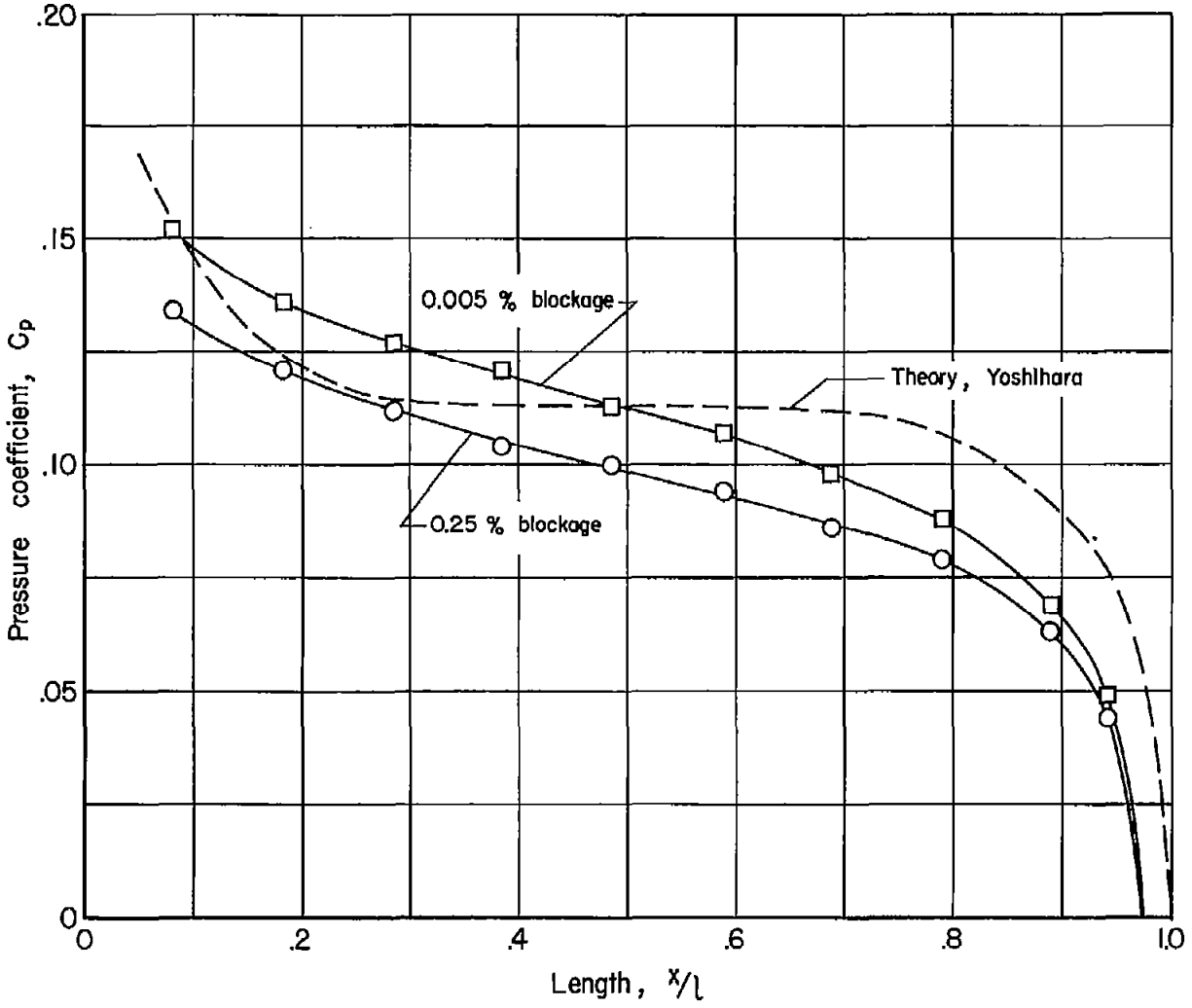

Figure 9.- Pressure distribution on circular cone-cylinder at a Mach number of 1 at 0° angle of attack.

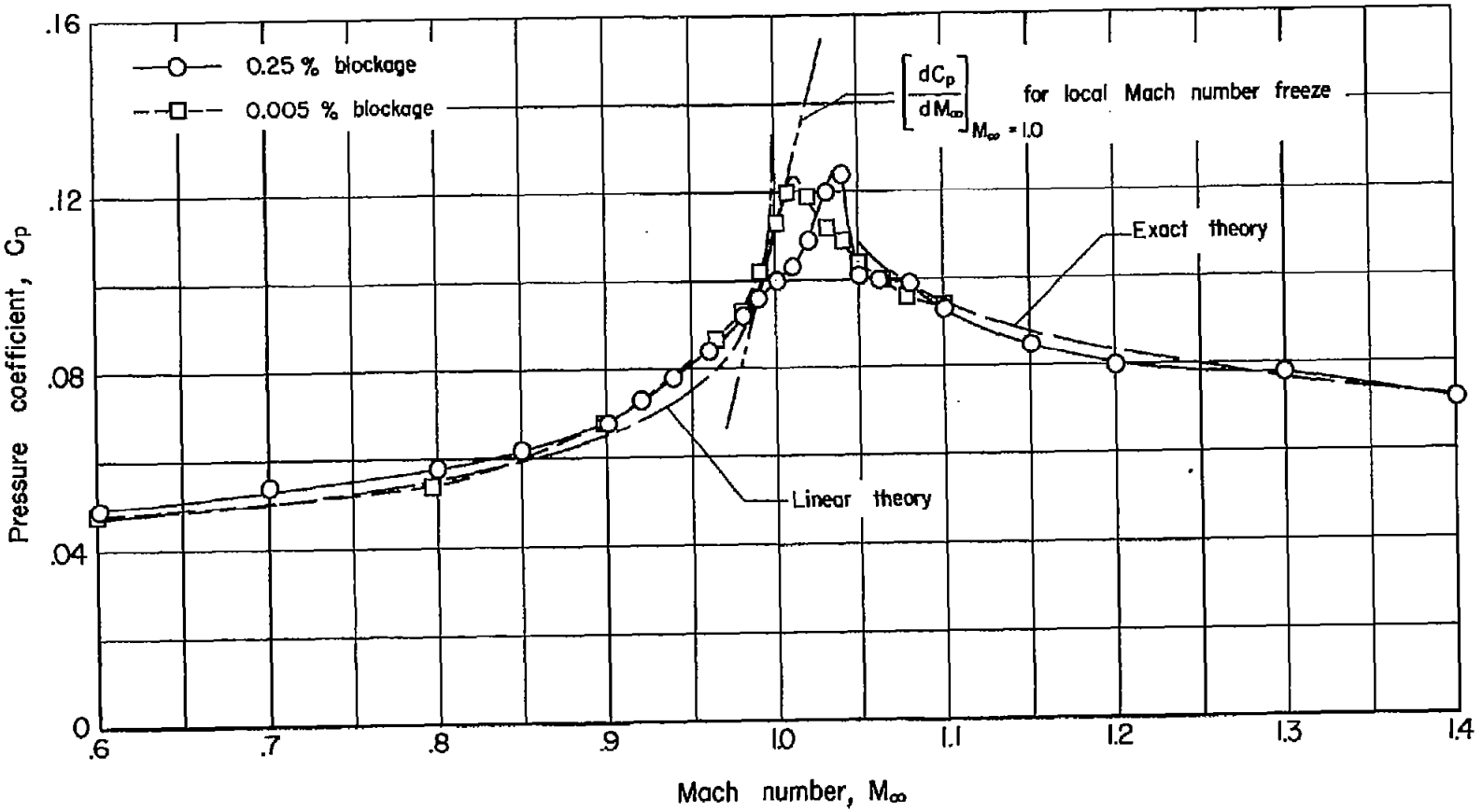

Figure 10.- Pressure distribution on circular cone-cylinder at $x/l = 0.486$ as a function of Mach number and at 0° angle of attack.

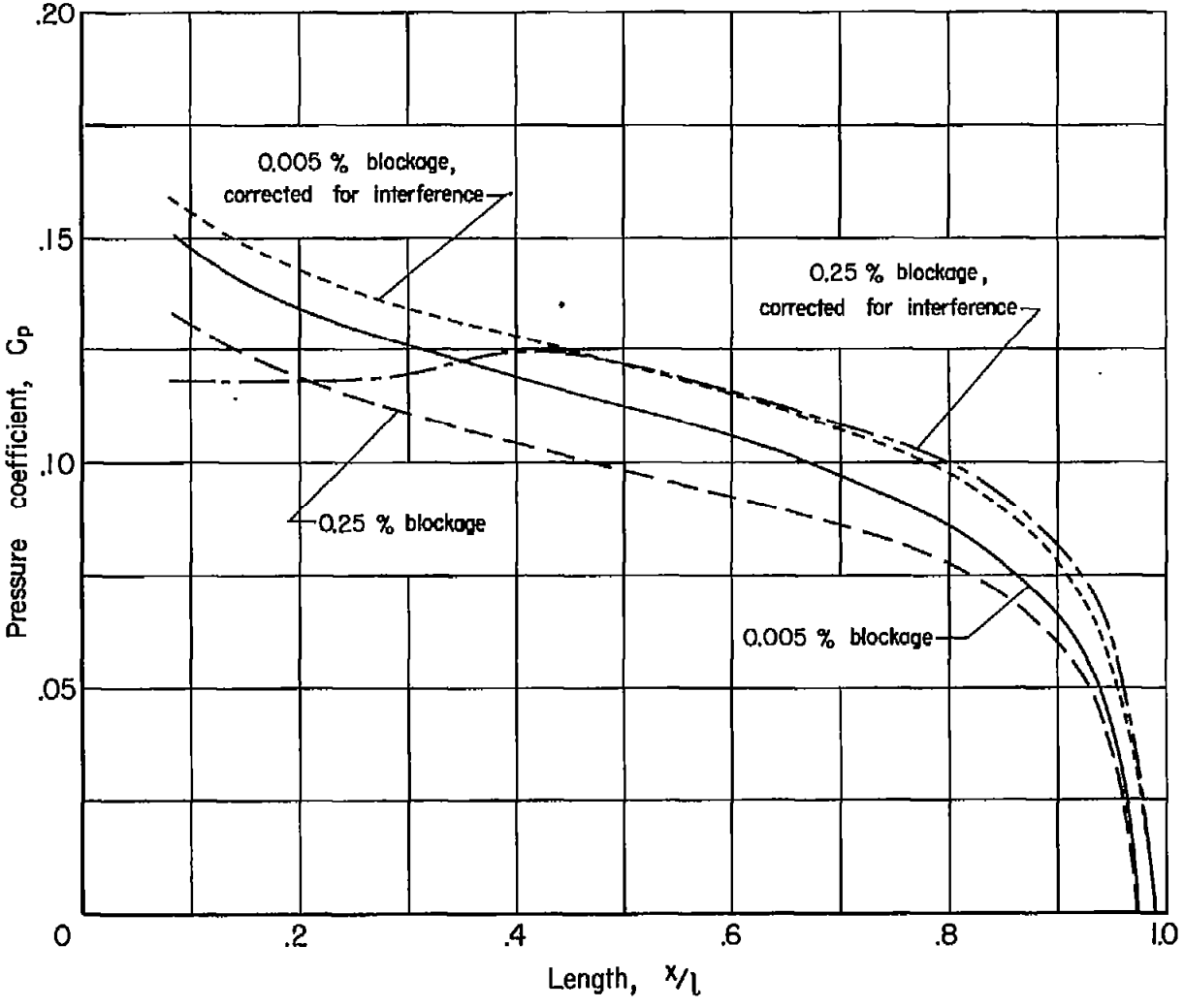

Figure 11.- Pressure distribution on circular cone-cylinder at a Mach number of 1 at 0° angle of attack.

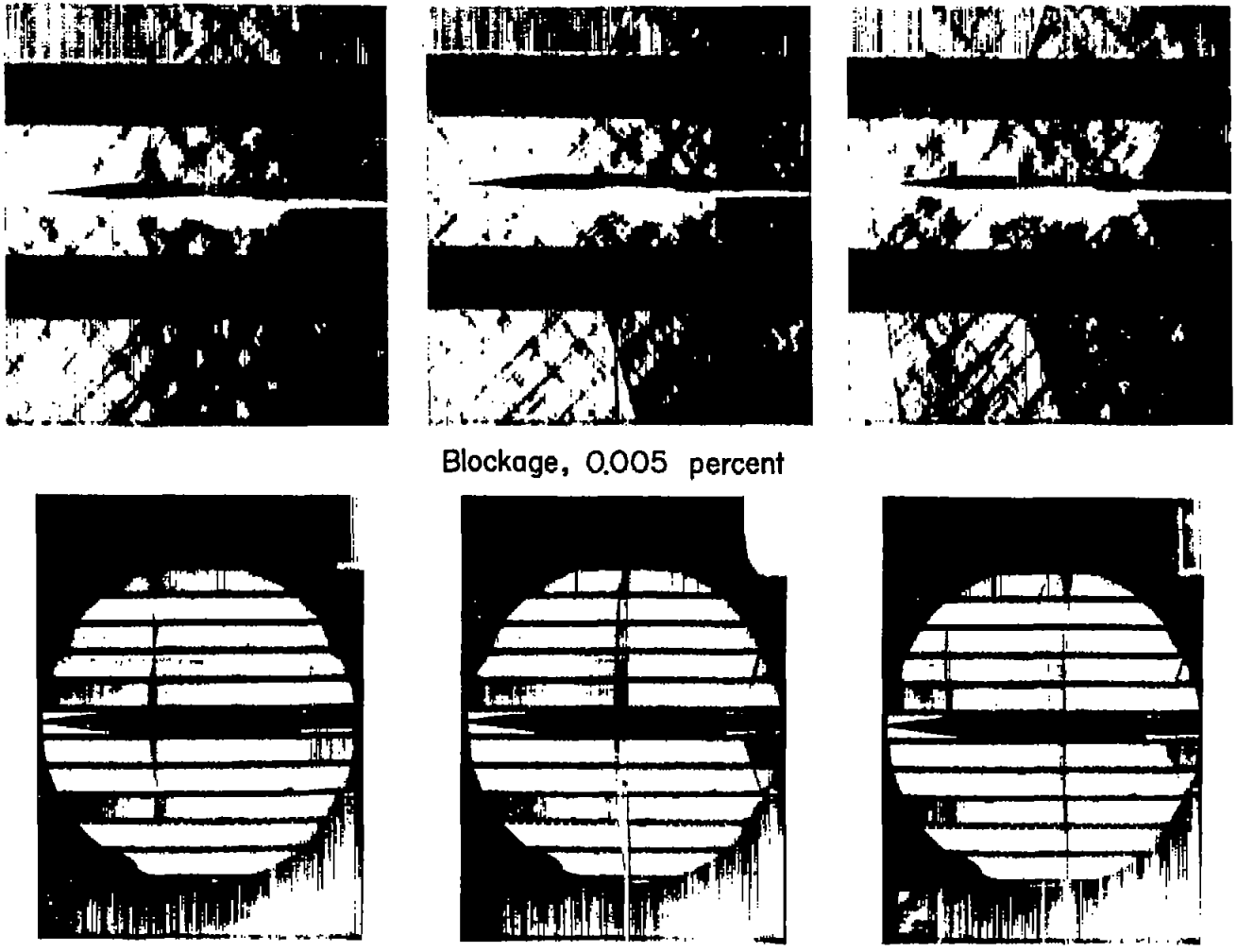

Figure 12.- Schlieren photographs of flow field about circular cone-cylinder in the two test facilities at transonic Mach numbers.

Blockage, 0.005 percent

Blockage, 0.25 percent

M_∞=1.04 M_∞=1.06 M_∞=1.10

Figure 12.- Concluded.